

Channel State Acquisition in Uplink NOMA for Cellular-Connected UAV: Exploitation of Doppler and Modulation Diversities

DONATELLA DARSENA¹ (SENIOR MEMBER, IEEE), IVAN IUDICE², AND FRANCESCO VERDE¹ (SENIOR MEMBER, IEEE)

¹Department of Electrical Engineering and Information Technology, University Federico II, Naples I-80125, Italy

²Reliability & Security Department, Italian Aerospace Research Centre (CIRA), Capua I-81043, Italy

CORRESPONDING AUTHOR: F. VERDE (e-mail: f.verde@unina.it).

This work was partially supported by the European Union under the Italian National Recovery and Resilience Plan (NRRP) of NextGenerationEU, partnership on "Telecommunications of the Future" (PE00000001 - program "RESTART") and the CIRA project "MATIM".

ABSTRACT

Integration of unmanned aerial vehicles (UAVs) for surveillance or monitoring applications into fifth generation (5G) New Radio (NR) cellular networks is an intriguing problem that has recently tackled a lot of interest in both academia and industry. For an efficient spectrum usage, we consider a recently-proposed sky-ground nonorthogonal multiple access (NOMA) scheme, where a cellular-connected UAV acting as aerial user (AU) and a static terrestrial user (TU) are paired to simultaneously transmit their uplink signals to a base station (BS) in the same time-frequency resource blocks. In such a case, due to the highly dynamic nature of the UAV, the signal transmitted by the AU experiences both time dispersion due to multipath propagation effects and frequency dispersion caused by Doppler shifts. On the other hand, for a static ground network, frequency dispersion of the signal transmitted by the TU is negligible and only multipath effects have to be taken into account. To decode the superposed signals at the BS through successive interference cancellation, accurate estimates of both the AU and TU channels are needed. In this paper, we propose channel estimation procedures that suitably exploit the different circular/noncircular modulation formats (*modulation diversity*) and the different almost-cyclostationarity features (*Doppler diversity*) of the AU and TU by means of widely-linear time-varying processing. Our estimation approach is semi-blind since Doppler shifts and time delays of the AU are estimated based on the received data only, whereas the remaining relevant parameters of the AU and TU channels are acquired relying also on the available training symbols, which are transmitted by the AU and TU in a nonorthogonal manner. Monte Carlo numerical results demonstrate that the proposed channel estimation algorithms can satisfactorily acquire all the relevant parameters in different operative conditions.

INDEX TERMS Almost-cyclostationarity, channel estimation, circular and noncircular modulations, doubly selective channels, Doppler diversity, 5G New Radio (NR), modulation diversity, non-orthogonal multiple access (NOMA), unmanned aerial vehicles (UAVs), uplink.

I. Introduction

WITH the development of unmanned aerial vehicles (UAVs), computer vision, and sensor technology,

UAV systems have been increasingly employed in civilian and commercial applications, such as surveillance and monitoring, due to their ability to quickly cover large and difficult-to-reach areas. The recently-introduced concept of cellular-connected UAVs [1]–[3] represents a viable strategy

to integrate UAVs in fifth generation (5G) New Radio (NR) networks, by allowing them to transmit data to the cellular network as aerial users (AUs). 3GPP Release 18 is introducing 5G NR support to enhance the safe use of UAVs for commercial and leisure applications. Nevertheless, the integration of UAVs into cellular networks introduces two interrelated basic challenges [4], [5]. First, existing 5G cellular infrastructures are designed to serve terrestrial users (TUs) and, thus, the antennas of the base stations (BSs) look downward: such a tilting might cause AUs to be served by the side lobes of the BSs and, consequently, they suffer from a reduction in antenna gain. Second, due to their mobility capabilities, AUs have more versatile movements than TUs, thereby introducing Doppler (frequency) shifts, which result in carrier frequency offset, inter-carrier interference, and reduced channel coherence time.

The feasibility of using existing cellular networks to support UAVs in the low-altitude airspace has been demonstrated in [6]–[8]. Specifically, it has been shown that the favorable line-of-sight (LoS) propagation conditions for UAVs flying in the sky can compensate for the reduced gain of antenna side lobes of the BSs, provided that UAVs fly below 120–200 m. A first consequence of flying at lower altitudes is that the AU-to-BS channel exhibits multipath components (MPCs) consisting of an LoS link with high probability and a cluster of reflected, delayed paths [9]. Severe Doppler shifts are caused by the high carrier frequency and high velocity of the UAV, and they are influenced by the angular distribution of the scattered components. Indeed, different MPCs may have largely different Doppler shifts.

To support AUs in cellular networks, there are two possible multiple access schemes. In the case of orthogonal multiple access (OMA) [10]–[19], AUs and TUs are served using orthogonal resource blocks (RBs). On the other hand, *non-orthogonal multiple access (NOMA)* allows AUs and TUs to simultaneously share the same spectrum through power-domain or code-domain multiplexing: in this case, successive interference cancellation (SIC) is used at the BS to separate the signals. In many cases, NOMA ensures superior spectral efficiency with respect to OMA [20]–[25].

A. NOMA for cellular-connected UAVs

Outage probabilities in downlink and uplink NOMA transmissions have been evaluated in [26] based on instantaneous distinct signal power for devices including UAVs. In [27], an aerial-ground NOMA scheme that pairs the AU and TU for data and control links has been investigated, by exploiting the asymmetric features of the channels and rate demands of the AU and TU in the downlink communication. The authors in [28] have proposed a cooperative downlink NOMA scheme to cancel co-channel interference via SIC in ideal two-cell networks. A cooperative NOMA scheme that exploits existing backhaul links among BSs for SIC operations has been proposed in [29]. An uplink NOMA has been proposed in [30] to serve AU and TU, where AU

trajectory and its cell-association order are jointly optimized, whereas the use of uplink NOMA for AUs and TUs has been studied via stochastic geometry, where the mobility of the AUs is taken into account. The probability that the achievable data rate of both the AU and TU exceeds the respective target rates is calculated in [31], where the minimum height that the AU needs to fly, at each transmission point along the given trajectory, is also numerically determined in order to satisfy a certain quality of service constraint. Finally, the authors in [32] have derived the optimal precoding that maximizes the uplink sum-rate of an AU and multiple TUs.

A common underlying approach of all the aforementioned works [26]–[32] is that Doppler shifts due to the UAV motions are a cause of performance degradation rather than a source of diversity. Indeed, it is tacitly assumed that large Doppler shifts have been previously compensated for or, as in [31], that the AU transmits its data to the BS by maintaining a fixed position over selected points along a given trajectory (i.e., transmission during hovering flight). However, compensation of Doppler shifts is a challenging task in multipath channels, except for the case when the MPCs of the AU-to-BS channel have a very similar Doppler shift, which is a situation that may not be fulfilled in the low-altitude airspace [9]. Moreover, allowing the UAV to transmit only in the hovering-flight state along its trajectory entails a waste of both communication and power resources. *Another shortcoming of the aforementioned papers [26]–[32] is that channel estimation issues have not been accounted at all.* In a NOMA setting, channel acquisition of both the AU and TU channels is crucial to obtain accurate SIC at the BS.

B. Modulation formats for double-selective channels

The choice of the digital modulation format crucially determines accuracy and signaling overhead of channel estimation. *Orthogonal time frequency space (OTFS)* and *orthogonal frequency division multiplexing (OFDM)* are digital modulation formats designed to handle doubly (i.e., time- and frequency) selective channels. OFDM modulation directly places symbols in the time-frequency (TF) domain, whereas OTFS is a modulation technique in which symbols are transmitted in the delay-Doppler (DD) domain [33].

OFDM is immune to the frequency-selective nature of the wireless channel. However, if frequency dispersion is also introduced by the channel in the form of Doppler shifts, the orthogonality of the subcarriers is destroyed, thus resulting in intercarrier interference (ICI). On the other hand, OTFS might cope with multipath fading and Doppler shifts more effectively, but such a robustness comes at the cost of a nonnegligible increase in signal processing complexity.

OTFS modulation has been used in [34] for the implementation of NOMA among users with different mobility profiles: specifically, a high-mobility user is allowed to share the spectrum with multiple low-mobility NOMA users. Although the specific case of an AU is not explicitly considered in [34], [35], their framework may be adapted to the scenario

of cellular-connected UAVs, by regarding the high-mobility user as an UAV. However, perfect channel knowledge is assumed in [34], [35].

The accuracy and signaling overhead of channel estimation techniques for OTFS modulation strictly depend on the values assumed by the delays and Doppler shifts. Indeed, in the case of integer delays and Doppler shifts, the received symbol corresponding to a given channel path is well-localized in the corresponding DD bin [34]–[36]. On the other hand, for fractional delays and Doppler shifts, each transmitted symbol spreads into adjacent bins, resulting in received symbols interfering with each other [37]. Such an inter-path interference (IPI) is a source of performance degradation for channel estimation performed directly in the DD domain. In the case of training-based channel identification, which consists into placing pilot symbols in the DD grid, one way to reduce the detrimental effects of IPI is to introduce guard symbols [38]. However, the guard interval of the pilots needs to include the entire Doppler domain within the range of the maximum delay, which results in a large pilot overhead. To avoid waste of communication resources, cancellation procedures of IPI might be carried out before channel estimation [37], [39], which inevitably increase implementation complexity of OTFS coherent reception.

Channel estimation for OFDM modulation is directly performed in the TF domain and, with respect to OTFS, it can face with fractional delays and Doppler shifts more effectively. Moreover, OFDM was extensively used in many standards of wireless systems, e.g., digital audio/video broadcasting (DAB/DVB), Wi-Fi local networks, worldwide interoperability for microwave access (WiMAX), long term evolution (LTE) and LTE-Advanced, and, it has been adopted in the 5G NR network. OFDM is still considered one of the potential candidates for beyond-5G communication systems. However, since OFDM is more sensitive to Doppler shifts than OTFS, a higher level of estimation accuracy is demanded. Despite the fact that channel estimation for OFDM is a well-investigated topic, to the best of our knowledge, there are no effective channel estimation methods available yet for NOMA aerial and terrestrial OFDM uplink channels.

C. Contribution and organization

We consider a NOMA uplink scheme, which is referred to as *sky-ground (SG) NOMA*, where a flying AU is paired with a static (i.e., fixed) TU. The AU and TU have different propagation conditions and their received power can be rather different at the BS, regardless of their transmit power: indeed, the air-to-cellular (A2C) channel between the AU and the elevated terrestrial BS is doubly selective with significant Doppler shifts,¹ whereas the TU-to-BS channel is predominately frequency-selective with negligible Doppler effects. We propose to *exploit* the different mobile profiles of the AU and TU rather than to *counteract* the Doppler effects

¹The air-to-cellular channel is different from the air-to-ground one due to the non-negligible height of terrestrial BSs.

induced by the mobility of the UAV. In particular, the AU is allowed to continuously transmit along all its trajectory.

To counteract the frequency-selectivity of both channels, the AU and TU resort to the OFDM transmission format. To improve the user separation capability of the BS, we propose to exploit a further source of diversity between the two users in the modulation domain: in both training (or pilot) and data phases, the TU transmits *circular* symbols, whereas the AU employs *noncircular* modulation.

Acquisition of channel state information (CSI) in uplink NOMA is a challenging task, since channel estimation in current wireless data communications standards is mainly based on training sequences sent from the users to the BS that are orthogonal in either time or frequency domain. Orthogonal RBs for training adversely affect spectral efficiency and system performance, especially in the uplink. We consider a nonorthogonal training scheme where the training data of one user is contaminated by either the pilots or the information-bearing data of the other user. In this challenging scenario, we propose a two-stage approach: first, the channel parameters of the AU are semi-blindly estimated by also exploiting the *almost-cyclostationarity (ACS) properties* [40] of the received signal that depend on the Doppler shifts of the AU-to-BS channel (*Doppler diversity*), as well as the different circular/noncircular features of the AU and TU (*modulation diversity*); subsequently, capitalizing on the CSI knowledge of the AU, the overall channel of the TU is acquired with a pilot-aided improved widely-linear (WL) estimator [41]. The performances of the proposed channel estimation algorithms are validated through extensive Monte Carlo numerical examples.

The paper is organized as follows. The system model of the considered uplink SG-NOMA is described in Section II. The proposed estimation strategies for the AU and TU are developed in Sections III and IV, respectively. Monte Carlo numerical results are reported in Section V in terms of channel estimation accuracy. Finally, the main results obtained in the paper are summarized in Section VI.

D. Basic notations

Upper- and lower-case bold letters denote matrices and vectors; the superscripts $*$, T , H , and -1 denote the conjugate, the transpose, the Hermitian (conjugate transpose), and the inverse of a matrix; \mathbb{C} , \mathbb{R} and \mathbb{Z} are the fields of complex, real and integer numbers; \mathbb{C}^n [\mathbb{R}^n] denotes the vector-space of all n -column vectors with complex [real] coordinates; similarly, $\mathbb{C}^{n \times m}$ [$\mathbb{R}^{n \times m}$] denotes the vector-space of all the $n \times m$ matrices with complex [real] elements; $\delta(\tau)$ is the Dirac delta; δ_n is the Kronecker delta, i.e., $\delta_n = 1$ when $n = 0$ and zero otherwise; $j \triangleq \sqrt{-1}$ denotes the imaginary unit; $\max(x, y)$ [$\min(x, y)$] returns the maximum [minimum] between $x \in \mathbb{R}$ and $y \in \mathbb{R}$; $\lfloor x \rfloor$ rounds $x \in \mathbb{R}$ to the nearest integer less than or equal to x ; the (linear) convolution operator is denoted with $*$; $\frac{\partial}{\partial x^*} f$ is the complex derivative of the real-valued scalar function f with respect to x^* [42]; $\mathbf{0}_n$,

$\mathbf{O}_{n \times m}$ and \mathbf{I}_n denote the n -column zero vector, the $n \times m$ zero matrix and the $n \times n$ identity matrix; \mathbf{J}_n is given by

$$\mathbf{J}_n \triangleq \begin{pmatrix} \mathbf{O}_{n \times n} & \mathbf{I}_n \\ \mathbf{I}_n & \mathbf{O}_{n \times n} \end{pmatrix} \in \mathbb{R}^{(2n) \times (2n)}; \quad (1)$$

$\{\mathbf{a}\}_\ell$ is the ℓ th entry of $\mathbf{a} \in \mathbb{C}^n$; $\{\mathbf{A}\}_{\ell,\ell}$ and $\text{trace}(\mathbf{A})$ denote the ℓ th diagonal entry and the trace of $\mathbf{A} \in \mathbb{C}^{n \times n}$; $\text{rank}(\mathbf{A})$ is the rank of $\mathbf{A} \in \mathbb{C}^{n \times m}$; \otimes is the Kronecker product; $\|\mathbf{A}\| \triangleq [\text{tr}(\mathbf{A}\mathbf{A}^H)]^{1/2}$ denotes the Frobenius norm of $\mathbf{A} \in \mathbb{C}^{n \times m}$ [43]; $\mathbf{A} = \text{diag}(a_0, a_1, \dots, a_{n-1}) \in \mathbb{C}^{n \times n}$ is diagonal; $\langle \cdot \rangle$ represents infinite-time temporal averaging and $\mathbb{E}[\cdot]$ denotes ensemble averaging; $[\cdot]_2$ stands for modulo-2 operation; finally, with denote with $x(t)$ and $x[n]$ continuous-time and discrete-time signals, respectively.

E. Special functions and matrices

The Dirichlet (or periodic sinc) function is defined as

$$D_n(x) \triangleq \frac{\sin(\pi x n)}{\sin(\pi x)} e^{-j\pi(n-1)x} \quad (2)$$

for each $x \in \mathbb{R}$. $\mathbf{W}_n \in \mathbb{C}^{n \times n}$ is the unitary symmetric n -point inverse discrete Fourier transform (IDFT) matrix, whose $(m+1, p+1)$ -th entry is given by $\frac{1}{\sqrt{n}} e^{j\frac{2\pi}{n}mp}$ for $m, p \in \{0, 1, \dots, n-1\}$, and its inverse $\mathbf{W}_n^{-1} = \mathbf{W}_n^H$ is the n -point discrete Fourier transform (DFT) matrix; $\mathbf{F} \in \mathbb{R}^{P \times P}$ and $\mathbf{B} \triangleq \mathbf{F}^T \in \mathbb{R}^{P \times P}$ denote the *forward shift* and *backward shift* matrices, whose first column and the first row are given by $[0, 1, 0, \dots, 0]^T$ and $[0, 1, 0, \dots, 0]$, respectively.

II. System model and basic assumptions

The considered single-cell network scenario encompasses an elevated BS, mobile AUs, and static TUs. The BS is located within the cell at a fixed height H_{BS} , whereas the AU flies at an altitude H_A above the ground.² We restrict ourselves to uplink communications since advanced signal detection algorithms of NOMA are more affordable at the BS [25]. A uniform linear array (ULA) is used at the BS with J antennas. The AUs are represented by single-antenna UAVs that are employed for surveillance or monitoring a given area within a cell and transmit data to the corresponding BS over given A2C links. According to 5G NR channel access schemes for terrestrial cellular networks [44], we assume that TUs transmit to the BS using the OMA scheme and, hence, there is no interference among the TUs in the cell. The extension of the proposed approach to the case in which nonorthogonal RBs are assigned to TUs in the uplink is discussed in Subsections III-D and IV-B.

In this paper, we consider an uplink SG-NOMA protocol, where single-antenna TUs share their RBs with the AUs. As in [31], we assume that each AU is randomly paired with a different static (i.e., fixed) TU (see Fig. 1). Hence, the scenario of interest boils down to the case of a single

²The proposed estimation algorithms can be straightforwardly modified to account for the case where the AU varies its height along the trajectory.

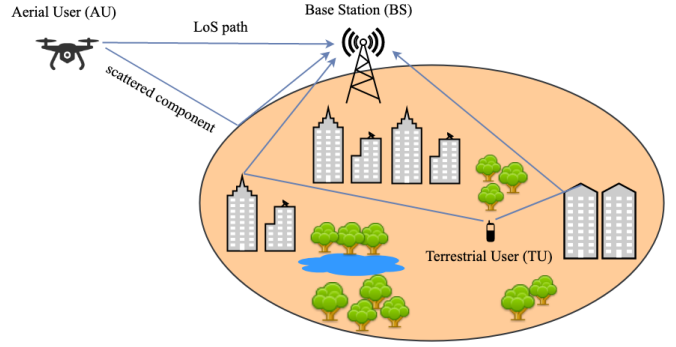


FIGURE 1. Uplink sky-ground NOMA: the UAV and the terrestrial user transmit their own uplink signals to the BS in the same RBs.

AU and a paired TU.³ The two-user scenario represents the case of major practical interest for NOMA, since it results in acceptable interference levels [45]. Moreover, we assume that inter-cell interference (ICI) coordination techniques are employed to mitigate terrestrial ICI [46], [47]. When the UAV flies in the low-altitude airspace [6]–[8], the LoS probability between the UAV and the neighboring co-channel BSs may be very low and ICI coordination (ICIC) only needs to involve a few BSs in a local region to exchange control information via high-speed backhaul links. In this case, the use of more sophisticated aerial-ground interference mitigation/cancellation procedures [3] might be avoided. Additionally, since each AU uses NOMA with a paired TU in the same cell, terrestrial ICIC indirectly limits aerial-ground interference between the UAV and co-channel terrestrial communications. Thus, in this work, we focus on the equivalent scenario with a single BS and a single AU-TU pairing in a given cell, without ICI.

A. Transmit signal model

Both users employ OFDM transmission to cope with the time-dispersive nature of the channel.

The independent symbol streams emitted by the AU and the TU ($n \in \mathbb{Z}$) are denoted with $\{s_A[n]\}$ and $\{s_T[n]\}$, respectively.⁴ We model $\{s_A[n]\}$ as a sequence of zero-mean unit-variance independent and identically distributed (i.i.d.) complex *noncircular* random variables [48], with second-order moment $\mathbb{E}(s_A^2[n]) \neq 0$. On the other hand, $\{s_T[n]\}$ is modeled as a sequence of zero-mean unit-variance i.i.d. complex *circular* random variables, i.e., $\mathbb{E}(s_T^2[n]) = 0$. 5G NR has been natively designed for circular modulation schemes, such as phase shift keying (PSK) and quadrature amplitude modulation (QAM). Noncircular modulation

³In principle, multiple AUs can be paired with a single static TU. In this case, the proposed estimation framework might be extended straightforwardly, provided that the superimposed AU signals exhibit different ACS properties at the BS, i.e., the AU-to-BS channels are characterized by different Doppler shifts.

⁴Throughout the paper, the subscripts A and T refer to the AU (i.e., UAV) and the TU, respectively.

schemes have been subsequently introduced for the uplink data channel (physical uplink shared channel - PUSCH) and control channel (physical uplink control channel - PUCCH) transmissions [49]–[51], such as $\pi/2$ binary PSK (BPSK). These waveforms, when combined with an appropriate spectrum shaping, enable low peak-to-average-power ratio transmissions without compromising the error rate performance, which is a desirable property for UAV communications. We will show herein that exploitation of the different second-order statistics (i.e., noncircular versus circular) of the AU and TU signals is instrumental into acquiring CSI in NOMA.

Both users share the same M orthogonal subcarriers. Let $s_{\text{TX}}^{[m]}[\ell] \triangleq s_{\text{TX}}[\ell M + m]$ represent the symbol transmitted in the ℓ th data block on the m th subcarrier, with $\text{TX} \in \{\text{A}, \text{T}\}$, the vector $\mathbf{s}_{\text{TX}}[n] \triangleq (s_{\text{TX}}^{[0]}[n], s_{\text{TX}}^{[1]}[n], \dots, s_{\text{TX}}^{[M-1]}[n])^T \in \mathbb{C}^M$ is subject to IDFT and cyclic prefix (CP) insertion, thus yielding $\mathbf{u}_{\text{TX}}[n] \triangleq (u_{\text{TX}}^{[0]}[n], u_{\text{TX}}^{[1]}[n], \dots, u_{\text{TX}}^{[P-1]}[n])^T = \mathbf{I}_{\text{cp}} \mathbf{W}_M \mathbf{s}_{\text{TX}}[n]$, where $\mathbf{I}_{\text{cp}} \in \mathbb{R}^{P \times M}$ models the insertion of a CP of length L_{cp} , with $P \triangleq M + L_{\text{cp}}$, and \mathbf{W}_M is the M -point IDFT (see Subsection I-D). The precoded data vector $\mathbf{u}_{\text{TX}}[n]$ undergoes parallel-to-serial (P/S) conversion, and the resulting data sequence $\{u_{\text{TX}}[\ell]\}$ feeds a digital-to-analog converter (DAC), operating at rate $1/T_c = P/T_s$, where $u_{\text{TX}}[\ell P + q] = u_{\text{TX}}^{[q]}[\ell]$, for $q \in \{0, 1, \dots, P-1\}$, the OFDM symbol period is T_s , whereas T_c is the sampling period. The baseband transmitted continuous-time signal at the output of the DAC is given by

$$x_{\text{TX}}(t) = \sum_{\ell=-\infty}^{+\infty} \sum_{q=0}^{P-1} u_{\text{TX}}^{[q]}[\ell] \psi_{\text{DAC}}(t - qT_c - \ell T_s) \quad (3)$$

for $\text{TX} \in \{\text{A}, \text{T}\}$, where $\psi_{\text{DAC}}(t)$ denotes the impulse response of the DAC.

B. Channel model for terrestrial user

The far-field channel between the TU and the BS is invariant over a coherence time $T_{\text{coh}} \triangleq N_{\text{coh}} T_s$, with $N_{\text{coh}} \gg 1$, wherein it can be modeled as a *linear time invariant (LTI)* system with impulse response:

$$\mathbf{h}_{\text{T}}(\tau) = \sum_{k=1}^{K_{\text{T}}} g_{\text{T},k} \delta(\tau - \tau_{\text{T},k}) \mathbf{a}(\theta_{\text{T},k}) \quad (4)$$

where K_{T} is the number of paths between the terrestrial user and the BS, whereas $g_{\text{T},k}$, $\tau_{\text{T},k}$, and $\theta_{\text{T},k}$ denote the complex gain, the time delay, and the angle of arrival (AoA) at the BS of the k th path. Taking the first receive antenna as reference, the vector $\mathbf{a}(\theta) \in \mathbb{C}^J$ in (4) denotes the response vector of the BS in the direction $\theta \in [-\pi/2, \pi/2]$ relative to the boresight of the ULA and it is given by

$$\mathbf{a}(\theta) \triangleq \left(1, e^{j \frac{2\pi}{\lambda_{\text{carrier}}} d \sin(\theta)}, \dots, e^{j \frac{2\pi}{\lambda_{\text{carrier}}} (J-1) d \sin(\theta)} \right)^T \quad (5)$$

where d is the distance between two adjacent antennas and $\lambda_{\text{carrier}} = c/f_{\text{carrier}}$ is the wavelength, with c being the light speed. From now on, we will set $d = \lambda_{\text{carrier}}/2$ for simplicity.

Since each propagation path is approximately equal to the sum of independent micro-scatterers contributions, having

same time delay and AoA, the channel gains $\{g_{\text{T},k}\}$ can thus be modeled as independent zero-mean complex Gaussian random variables (*Rayleigh fading model*), with variances $\sigma_{\text{T},k}^2 \triangleq \mathbb{E}(|g_{\text{T},k}|^2)$, for $k \in \{1, 2, \dots, K_{\text{T}}\}$. It can be adopted for $\sigma_{\text{T},k}^2$ the common propagation model (see, e.g., [52])

$$\sigma_{\text{T},k}^2 = \sigma_{\text{T,ref}}^2 \mathcal{P}_{\text{T}} G_{\text{T}} G_{\text{BS,T}} \left(\frac{d_{\text{T,ref}}}{d_{\text{T},k}} \right)^{\eta_{\text{T}}} \quad (6)$$

where $\sigma_{\text{T,ref}}^2$ is a unitless constant, \mathcal{P}_{T} is the transmit power of the TU, G_{T} and $G_{\text{BS,T}}$ represent the antenna gains of the TU and the BS, respectively, $d_{\text{T},k}$ denotes the propagation length along the k -th path, $d_{\text{T,ref}}$ is a reference distance for the antenna far field, and η_{T} is the path-loss exponent.

C. Channel model for the aerial user

For A2C link, we assume a two-ray channel model,⁵ which includes the LoS path and a scattered (i.e., non-LoS) component [9] (see also Fig. 1). The non-LoS (NLoS) component is physically due to many rays reflected or scattered from closely-spaced terrestrial obstacles within the vicinity of the BS, which are characterized by a very narrow beamwidth [9] and appear grouped or “clustered” in delay for sufficiently high elevation angles [54]. Henceforth, such rays are expected to have a very similar Doppler shift, as they all come from similar directions (narrow beamwidth), and a very similar delay (high elevation angle). Assuming that the UAV is moving (relative to the BS) at constant *radial* speed v within the observation interval $[0, T_0)$, with $T_0 \triangleq N_0 T_s \leq T_{\text{coh}}$, under the customary assumption that the communication bandwidth $B \sim 1/T_c$ is much smaller than the carrier frequency f_{carrier} , the far-field low-pass equivalent *linear time-varying (LTV)* time-delay impulse response of the UAV-to-BS channel can be expressed as⁶ (see, e.g., [53])

$$\mathbf{h}_{\text{A}}(t, \tau) = g_{\text{A,L}} e^{j 2\pi f_{\text{A,L}} t} \delta(\tau - \tau_{\text{A,L}}) \mathbf{a}(\theta_{\text{A,L}}) + g_{\text{A,N}} e^{j 2\pi f_{\text{A,N}} t} \delta(\tau - \tau_{\text{A,N}}) \mathbf{a}(\theta_{\text{A,N}}) \quad (7)$$

where $g_{\text{A,L}}$ [$g_{\text{A,N}}$], $\theta_{\text{A,L}}$ [$\theta_{\text{A,N}}$], $\tau_{\text{A,L}}$ [$\tau_{\text{A,N}}$], $f_{\text{A,L}} = f_{\text{max}} \cos(\vartheta_{\text{A,L}})$ [$f_{\text{A,N}} = f_{\text{max}} \cos(\vartheta_{\text{A,N}})$] are the complex (i.e., amplitude and phase) path gain, the AoA at the BS, the time delay, and the Doppler shift of the LoS [NLoS] component, with $\vartheta_{\text{A,L}} \in [0, \pi]$ [$\vartheta_{\text{A,N}} \in [0, \pi]$] representing the angle of departure (AoD) of the LoS [NLoS] ray relative to the direction of motion of the UAV and $f_{\text{max}} \triangleq f_{\text{carrier}} v/c \ll B$. It is noteworthy that the LTV model (7) is justified by the fact that the UAV is allowed to communicate with the BS while it is flying and, hence, we do not constrain the UAV to transmit only in the hovering-flight state as, e.g., in [31].

Since the speed and physical location of the UAV would change much slower than the symbol period T_s , the UAV

⁵The proposed estimation framework can be extended to the multi-ray case for the A2C channel. However, for blind identification of the corresponding channel parameters, the Doppler shifts of the different rays have to fulfill a mild technical condition to avoid ambiguities [53].

⁶Throughout the paper, the subscripts L and N indicate parameters referring to the LoS and NLoS components of the AU, respectively.

related parameters $g_{A,L}$, $g_{A,N}$, $\theta_{A,L}$, $\theta_{A,N}$, $\tau_{A,L}$, $\tau_{A,N}$, $f_{A,L}$, and $f_{A,N}$ can be assumed as unchanged within $N_0 \leq N_{\text{coh}}$ OFDM symbol blocks. Local stationarity of the scattering geometry is widely used in the literature and experimentally confirmed in [55]. Moreover, we consider an underspread A2C channel, characterized by $\max\{\tau_{A,L}, \tau_{A,N}\} f_{\text{max}} \ll 1$, which is true for many wireless channels [56].

The statistical characterization of (7) is herein determined by assuming that the A2C channel is LoS with probability one.⁷ Specifically, the gain $g_{A,L}$ is deterministic and takes the value $\sigma_{A,L} e^{j\phi_{A,L}}$. The parameter $\phi_{A,L} \in [0, 2\pi)$ accounts for a (possible) phase misalignment along the LoS path between the UAV and the BS. On the other hand, the NLoS gain $g_{A,N}$ is modeled as a complex circular zero-mean Gaussian random variable with variance $\sigma_{A,N}^2 \triangleq \mathbb{E}(|g_{A,N}|^2)$. Similarly to (6), for $C \in \{L, N\}$, $\sigma_{A,L}^2$ and $\sigma_{A,N}^2$ can be modeled as

$$\sigma_{A,C}^2 = \sigma_{A,C,\text{ref}}^2 \mathcal{P}_A G_A G_{\text{BS},A,C} \left(\frac{d_{A,\text{ref}}}{d_{A,C}} \right)^{\eta_{A,C}} \quad (8)$$

where $\sigma_{A,C,\text{ref}}^2$ is unitless, \mathcal{P}_A is the transmit power of the AU, G_A and $G_{\text{BS},A,C}$ represent the antenna gains of the AU and the BS, respectively, $d_{A,C,\text{ref}}$ is a reference distance for the antenna far field, $d_{A,C}$ denotes the propagation length of path $C \in \{L, N\}$, and $\eta_{A,C}$ is the corresponding path-loss exponent. It should be observed that the UAV-to-BS channel is described by a *Rician fading model*, whose corresponding Rician factor is $K_A \triangleq \sigma_{A,L}^2 / \sigma_{A,N}^2$. We underline that the path $C \in \{L, N\}$ of the AU and the MPCs of the TU see different BS antenna gains $G_{\text{BS},A,C}$ and $G_{\text{BS},T}$, respectively, which reflects the fact that the AU and TU may be served by different lobes of the BS antennas.

D. Receive signal model before CP removal

Hereinafter, without loss of generality, the reported signal models refer to the observation interval $[0, T_0)$ of the TU channel, which corresponds to the transmission of N_0 OFDM symbols. After filtering, for $t \in [0, T_0)$ and $j \in \{1, 2, \dots, J\}$, the baseband received signal at the j -th antenna of the BS can be written as

$$\begin{aligned} y_j(t) = & g_{A,L} e^{j2\pi f_{A,L}t} x_A(t - \tau_{A,L}) e^{j\pi(j-1)\sin(\theta_{A,L})} \\ & + g_{A,N} e^{j2\pi f_{A,N}t} x_A(t - \tau_{A,N}) e^{j\pi(j-1)\sin(\theta_{A,N})} \\ & + \sum_{k=1}^{K_T} g_{T,k} x_T(t - \tau_{T,k}) e^{j\pi(j-1)\sin(\theta_{T,k})} + w_j(t) \end{aligned} \quad (9)$$

where $w_j(t)$ is the complex envelope of (filtered) noise statistically independent of $x_{\text{TX}}(t)$, for $\text{TX} \in \{A, T\}$.

⁷It is shown in [31] that, by using the model and the parameters reported in [57]–[59] and assuming a practical UAV altitude range of 25–120 meters, the probability of occurrence of the LoS event between the UAV and the terrestrial BS is equal to one when either the horizontal distance of the UAV from the BS is smaller than about 75 meters or the elevation angle between the UAV and the BS is greater than 20 degrees.

If we denote with $\psi_{\text{ADC}}(t)$ the impulse response of the (anti-aliasing) filter at the input of the analog-to-digital converter (ADC) at the BS, the impulse response of the cascade of the DAC interpolation filter and the ADC antialiasing filter is given by $\psi(t) \triangleq \psi_{\text{DAC}}(t) * \psi_{\text{ADC}}(t)$, obeying $\psi(t) \equiv 0$ for $t \notin [0, L_{\text{filter}} T_c)$. The pulse $\psi(t)$ and its finite duration $L_{\text{filter}} T_c$ are known at the BS. A very common assumption in multicarrier applications is that $L_{\text{filter}} T_c + \tau_{\text{max}} < T_s$, with $\tau_{\text{max}} \triangleq \max(\tau_{A,L}, \tau_{A,N}, \tau_{T,1}, \dots, \tau_{T,K_T})$. Moreover, we customarily assume that the BS has been previously locked to the multipath component at (approximately) the minimum delay $\tau_{\text{min}} \triangleq \min(\tau_{A,L}, \tau_{A,N}, \tau_{T,1}, \dots, \tau_{T,K_T})$ and, without loss of generality, we set $\tau_{\text{min}} = 0$.

The signal (9) is sampled at $t_{n,p} \triangleq nT_s + pT_c$, for $n \in \mathbb{Z}$ and $p \in \{0, 1, \dots, P-1\}$. Let $y_j^{[p]}[n] \triangleq y_j(t_{n,p})$ be the discrete-time counterpart of (9), for $n \in \{0, 1, \dots, N_0-1\}$, one gets

$$\begin{aligned} y_j^{[p]}[n] = & g_{A,L} e^{j2\pi\nu_{A,L}(n+\frac{p}{P})} x_{A,L}^{[p]}[n] e^{j\pi(j-1)\sin(\theta_{A,L})} \\ & + g_{A,N} e^{j2\pi\nu_{A,N}(n+\frac{p}{P})} x_{A,N}^{[p]}[n] e^{j\pi(j-1)\sin(\theta_{A,N})} \\ & + \sum_{k=1}^{K_T} g_{T,k} x_{T,k}^{[p]}[n] e^{j\pi(j-1)\sin(\theta_{T,k})} + w_j^{[p]}[n] \end{aligned} \quad (10)$$

where $\nu_{A,C} \triangleq f_{A,C} T_s \in [-1/2, 1/2)$ is the *normalized Doppler shift* of the UAV relative to path $C \in \{L, N\}$, whereas

$$\begin{aligned} x_{A,C}^{[p]}[n] = & \sum_{\ell=n-1}^n \sum_{q=0}^{P-1} u_A^{[q]}[\ell] \\ & \cdot \alpha_{A,C} [(n-\ell)P + (p-q) - d_{A,C}] \end{aligned} \quad (11)$$

$$\begin{aligned} x_{T,k}^{[p]}[n] = & \sum_{\ell=n-1}^n \sum_{q=0}^{P-1} u_T^{[q]}[\ell] \\ & \cdot \alpha_{T,k} [(n-\ell)P + (p-q) - d_{T,k}] \end{aligned} \quad (12)$$

where

$$\alpha_{A,C}[h] \triangleq \psi(hT_c - \chi_{A,C}) \quad (h \in \mathbb{Z}) \quad (13)$$

$$\tau_{A,C} = d_{A,C} T_c + \chi_{A,C} \quad (14)$$

$$\alpha_{T,k}[h] \triangleq \psi(hT_c - \chi_{T,k}) \quad (15)$$

$$\tau_{T,k} = d_{T,k} T_c + \chi_{T,k} \quad (16)$$

with integer delays $d_{A,C}$ and $d_{T,k}$, and fractional delays $\chi_{A,C} \in [0, T_c)$ and $\chi_{T,k} \in [0, T_c)$, and $w_j^{[p]}[n] \triangleq w_j(t_{n,p})$.

By gathering the obtained samples of the received signal into $\bar{\mathbf{y}}_j[n] \triangleq (y_j^{[0]}[n], y_j^{[1]}[n], \dots, y_j^{[P-1]}[n])^T \in \mathbb{C}^P$ and accounting for (10), we obtain the following vector model

$$\begin{aligned} \bar{\mathbf{y}}_j[n] = & \bar{\mathbf{H}}_{A,j}^{(0)}[n] \mathbf{s}_A[n] + \bar{\mathbf{H}}_{A,j}^{(1)}[n] \mathbf{s}_A[n-1] \\ & + \bar{\mathbf{H}}_{T,j}^{(0)}[n] \mathbf{s}_T[n] + \bar{\mathbf{H}}_{T,j}^{(1)}[n] \mathbf{s}_T[n-1] + \bar{\mathbf{w}}_j[n] \end{aligned} \quad (17)$$

for $n \in \{0, 1, \dots, N_0 - 1\}$ and $j \in \{1, 2, \dots, J\}$, where

$$\begin{aligned} \bar{\mathbf{H}}_{A,j}^{(b)}[n] &\triangleq g_{A,L} \left(\mathbf{D}_{A,L} \mathbf{T}_{A,L}^{(b)} \boldsymbol{\Omega}_A \right) e^{j2\pi\nu_{A,L}n} e^{j\pi(j-1)\sin(\theta_{A,L})} \\ &\quad + g_{A,N} \left(\mathbf{D}_{A,N} \mathbf{T}_{A,N}^{(b)} \boldsymbol{\Omega}_A \right) e^{j2\pi\nu_{A,N}n} e^{j\pi(j-1)\sin(\theta_{A,N})} \end{aligned} \quad (18)$$

$$\bar{\mathbf{H}}_{T,j}^{(b)} \triangleq \sum_{k=1}^{K_T} g_{T,k} \left(\mathbf{T}_{T,k}^{(b)} \boldsymbol{\Omega}_T \right) e^{j\pi(j-1)\sin(\theta_{T,k})} \quad (19)$$

for $b \in \{0, 1\}$, with

$$\mathbf{D}_{A,C} \triangleq \text{diag}(1, e^{j\frac{2\pi}{P}\nu_{A,C}}, \dots, e^{j\frac{2\pi}{P}\nu_{A,C}(P-1)}) \quad (20)$$

for $C \in \{L, N\}$, whereas the $(p+1, q+1)$ th entry of the Toeplitz matrices $\mathbf{T}_{A,C}^{(b)} \in \mathbb{R}^{P \times P}$ and $\mathbf{T}_{T,k}^{(b)} \in \mathbb{R}^{P \times P}$ is given by $\alpha_{A,C}[bP + (p-q) - d_{A,C}]$ and $\alpha_{T,k}[bP + (p-q) - d_{T,k}]$, respectively, for $p, q \in \{0, 1, \dots, P-1\}$,

$$\boldsymbol{\Omega}_{TX} \triangleq \mathbf{I}_{cp} \mathbf{W}_M \in \mathbb{C}^{P \times M} \quad (21)$$

and $\bar{\mathbf{w}}_j[n] \triangleq (w_j^{[0]}[n], w_j^{[1]}[n], \dots, w_j^{[P-1]}[n])^T \in \mathbb{C}^P$ is a zero-mean complex circular Gaussian random vector with $\mathbb{E}(\bar{\mathbf{w}}_{j_1}[n_1] \bar{\mathbf{w}}_{j_2}^H[n_2]) = \sigma_w^2 \delta_{n_1-n_2} \delta_{j_1-j_2} \mathbf{I}_P$.

The signal model (17) before CP removal is used in Subsection III-A to blindly estimate the Doppler shifts and the time delays of the AU.

E. Receive signal model after CP removal

For $n \in \{0, 1, \dots, N_0 - 1\}$ and $j \in \{1, 2, \dots, J\}$, interblock interference (IBI) in (10) can be perfectly suppressed through CP removal, thus yielding, after DFT,

$$\begin{aligned} \mathbf{y}_j[n] &\triangleq \mathbf{W}_M^H \mathbf{R}_{cp} \bar{\mathbf{y}}_j[n] \\ &= \mathbf{H}_{A,j}[n] \mathbf{s}_A[n] + \mathbf{H}_{T,j} \mathbf{s}_T[n] + \mathbf{w}_j[n] \end{aligned} \quad (22)$$

provided that $L_{cp} \geq L_{\text{filter}} + \lceil \tau_{\text{max}}/T_c \rceil$, where $\mathbf{R}_{cp} \in \mathbb{R}^{M \times P}$ performs CP removal, $\mathbf{H}_{A,j}[n] \triangleq \mathbf{W}_M^H \mathbf{R}_{cp} \bar{\mathbf{H}}_{A,j}^{(0)}[n] \in \mathbb{C}^{M \times M}$ and $\mathbf{H}_{T,j} \triangleq \mathbf{W}_M^H \mathbf{R}_{cp} \bar{\mathbf{H}}_{T,j}^{(0)} \in \mathbb{C}^{M \times M}$, and, finally, the noise contribution is $\mathbf{w}_j[n] \triangleq \mathbf{W}_M^H \mathbf{R}_{cp} \bar{\mathbf{w}}_j[n] \in \mathbb{C}^M$. Moreover, accounting for (19), the matrix $\mathbf{H}_{T,j}$ can be written as reported at the top of the next page in (23), where the forward matrix $\mathbf{F} \in \mathbb{C}^{P \times P}$ has been defined in Subsection I-D and we have observed that the matrix in square brackets is circulant and, thus, it can be equivalently written as $\mathbf{W}_M \mathbf{M}_{T,j,k} \mathbf{W}_M^H$, with

$$\mathbf{M}_{T,j} \triangleq \sum_{k=1}^{K_T} \mathbf{M}_{T,j,k}. \quad (24)$$

The matrix $\mathbf{M}_{T,j,k} \triangleq \text{diag}(\boldsymbol{\mu}_{T,j,k})$ is diagonal, with

$$\boldsymbol{\mu}_{T,j,k} \triangleq \sqrt{M} \mathbf{W}_M^H \mathbf{L} \mathbf{g}_{T,j,k} \in \mathbb{C}^M \quad (25)$$

where

$$\mathbf{L} \triangleq (\mathbf{I}_{L_{cp}}, \mathbf{O}_{(M-L_{cp}) \times L_{cp}}^T)^T \in \mathbb{R}^{M \times L_{cp}} \quad (26)$$

$$\mathbf{g}_{T,j,k} \triangleq (\mathbf{0}_{d_{T,k}}^T, g_{T,k} e^{j\pi(j-1)\sin(\theta_{T,k})} \boldsymbol{\alpha}_{T,k}^T, \quad (27)$$

$$\dots, \mathbf{0}_{L_{cp}-L_{\text{filter}}-d_{T,k}-1}^T)^T \in \mathbb{C}^{L_{cp}} \quad (28)$$

$$\boldsymbol{\alpha}_{T,k} \triangleq (\alpha_{T,k}[0], \alpha_{T,k}[1], \dots, \alpha_{T,k}[L_{\text{filter}}])^T \in \mathbb{R}^{L_{\text{filter}}+1}. \quad (29)$$

On the other hand, the transmission of the AU is adversely affected by ICI due to the presence of Doppler shifts: in general, the channel matrix $\mathbf{H}_{A,j}[n]$ cannot be diagonalized through DFT.

By collecting the data received by all the antennas of the BS in the vector $\mathbf{y}[n] \triangleq (\mathbf{y}_1^T[n], \mathbf{y}_2^T[n], \dots, \mathbf{y}_J^T[n])^T \in \mathbb{C}^{JM}$, we obtain from (22) and (23) the signal model

$$\mathbf{y}[n] \triangleq \mathbf{H}_A[n] \mathbf{s}_A[n] + \mathbf{M}_T \mathbf{s}_T[n] + \mathbf{w}[n] \quad (30)$$

for $n \in \{0, 1, \dots, N_0 - 1\}$, where

$$\mathbf{H}_A[n] \triangleq (\mathbf{H}_{A,1}^T[n], \mathbf{H}_{A,2}^T[n], \dots, \mathbf{H}_{A,J}^T[n])^T \in \mathbb{C}^{(JM) \times M} \quad (31)$$

$$\mathbf{M}_T \triangleq (\mathbf{M}_{T,1}^T, \mathbf{M}_{T,2}^T, \dots, \mathbf{M}_{T,J}^T)^T \in \mathbb{C}^{(JM) \times M} \quad (32)$$

and $\mathbf{w}[n] \triangleq (\mathbf{w}_1^T[n], \mathbf{w}_2^T[n], \dots, \mathbf{w}_J^T[n])^T \in \mathbb{C}^{JM}$.

F. Nonorthogonal pilot allocation scheme

To acquire the channel parameters needed for demodulating the data (i.e., information-bearing) symbols transmitted by the users, the BS might rely on training (or pilot) symbols sent by both the AU and TU, over reserved time-frequency RBs in uplink. Specifically, we assume that user $\text{TX} \in \{A, T\}$ inserts $1 \leq Q_{\text{TX}} \leq M$ pilot symbols at distinct subcarrier locations

$$\begin{aligned} \mathcal{M}_{\text{TX}} &\triangleq \{m_{\text{TX},0}, m_{\text{TX},1}, \dots, m_{\text{TX},Q_{\text{TX}}-1}\} \\ &\subseteq \{0, 1, \dots, M-1\} \end{aligned} \quad (33)$$

during the $1 \leq N_{\text{TX,train}} \ll N_0$ distinct symbol intervals

$$\begin{aligned} \mathcal{N}_{\text{TX}} &\triangleq \{n_{\text{TX},1}, n_{\text{TX},2}, \dots, n_{\text{TX},N_{\text{TX,train}}}\} \\ &\subseteq \{0, 1, \dots, N_0-1\}. \end{aligned} \quad (34)$$

In NOMA schemes, the training phase of one user suffers from the interference generated by either the pilots or the data transmitted by the other one. Perfect separation of pilot symbols at the BS is possible only if the TU will not transmit neither pilots nor data on the set \mathcal{M}_A of subcarriers over the OFDM signaling intervals \mathcal{N}_A and vice versa. Obviously, besides requiring a stringent protocol-level cooperation between the aerial and terrestrial networks, such a latter strategy comes at a (possibly unaffordable) cost of spectral efficiency due to the time-varying nature of the AU channel and it is not considered herein.

III. Channel estimation for the aerial user

The task of the AU channel estimator is to provide to the WL-TV SIC filter the channel matrices $\mathbf{H}_{A,1}[n], \mathbf{H}_{A,2}[n], \dots, \mathbf{H}_{A,J}[n]$, for $n \in \{0, 1, \dots, N_0 - 1\}$. In this case, since the time-varying nature of the A2C channel prevents the diagonalization of $\mathbf{H}_{A,j}[n]$ through DFT, it is not possible to separate pilots and data symbols in the frequency-domain. For such a reason, we set $\mathcal{M}_A \equiv \{0, 1, \dots, M-1\}$ or, equivalently, $Q_A = M$, i.e., the AU inserts pilots at all the subcarriers within the symbol intervals specified by $\mathcal{N}_A = \{n_{A,1}, n_{A,2}, \dots, n_{A,N_{A,train}}\}$.

$$\mathbf{H}_{T,j} = \mathbf{W}_M^H \sum_{k=1}^{K_T} \underbrace{\left[g_{T,k} e^{j\pi(j-1)\sin(\theta_{T,k})} \sum_{\ell=0}^{L_{\text{filter}}} \alpha_{T,k}[\ell] \mathbf{R}_{\text{cp}} \mathbf{F}^{\ell+d_{T,k}} \mathbf{I}_{\text{cp}} \right]}_{\mathbf{W}_M \mathbf{M}_{T,j,k} \mathbf{W}_M^H} \mathbf{W}_M = \mathbf{M}_{T,j} \quad (23)$$

To reduce the amount of training, we propose a semi-blind approach to estimate the unknowns characterizing the channel matrices $\mathbf{H}_{A,1}[n], \mathbf{H}_{A,2}[n], \dots, \mathbf{H}_{A,J}[n]$. Specifically, Doppler and delay parameters are blindly estimated by exploiting the unique ACS properties of the signal transmitted by the AU, without relying on pilots. On the other hand, complex gain and AoA parameters are estimated by using the pilot symbols known by the BS. The estimators derived herein are based on the assumption that the AU channel parameters are deterministic but unknown quantities.

The proposed estimators of the AU channel parameters are summarized in Fig. 2.

A. Blind estimation of Doppler and delay parameters

The starting point of our blind estimation procedure is the signal (17), i.e., the *entire* OFDM block (including the CP) is processed for acquiring Doppler and delay parameters of the AU transmission. The ACS features of (17) stem from the fact that $\bar{\mathbf{H}}_{A,j}^{(b)}[n]$ in (18) is a discrete-time *almost-periodic* (AP) matrix [60] with (possibly) incommensurate frequencies $\{\nu_{A,L}, \nu_{A,N}\} \subseteq [-1/2, 1/2)$. Consequently, for $r \in \{-1, 0, 1\}$ and $j \in \{1, 2, \dots, J\}$, the correlation matrix $\mathbf{R}_{\bar{\mathbf{y}}_j \bar{\mathbf{y}}_j^*}[n, r] \triangleq \mathbb{E}(\bar{\mathbf{y}}_j[n] \bar{\mathbf{y}}_j^*[n-r]) \in \mathbb{C}^{P \times P}$ and its conjugate counterpart $\mathbf{R}_{\bar{\mathbf{y}}_j \bar{\mathbf{y}}_j^*}[n, r] \triangleq \mathbb{E}(\bar{\mathbf{y}}_j[n] \bar{\mathbf{y}}_j^T[n-r]) \in \mathbb{C}^{P \times P}$ are AP matrices, too, and the multivariate process (17) is said to be second-order wide-sense ACS [40].

Capitalizing on the fact that the AU transmits noncircular symbols while the TU adopts a circular modulation format (modulation diversity), the proposed blind estimation approach relies only on the conjugate second-order statistics of the ACS random process (17), which turn out to be free from both TU and noise contributions (a consequence of Doppler diversity). For $j \in \{1, 2, \dots, J\}$, one gets

$$\mathbf{R}_{\bar{\mathbf{y}}_j \bar{\mathbf{y}}_j^*}[n, r] = \sum_{C_1 \in \{L, N\}} \sum_{C_2 \in \{L, N\}} \Xi_{A,j,C_1,C_2}[r] \cdot e^{j2\pi(\nu_{A,C_1} + \nu_{A,C_2})n} \quad (35)$$

where the $P \times P$ matrices in (35) are defined in (36)–(38) at the top of the next page, with $\Delta \in \mathbb{C}^{M \times M}$ being a *known* diagonal matrix derived in the Appendix for the $\pi/2$ -BPSK case and depending on the noncircularity property of the AU symbols. Under mild regularity conditions, the AP matrix (35) can be equivalently written in terms of the generalized Fourier series expansion as follows

$$\mathbf{R}_{\bar{\mathbf{y}}_j \bar{\mathbf{y}}_j^*}[n, r] = \sum_{\alpha} \mathbf{R}_{\bar{\mathbf{y}}_j \bar{\mathbf{y}}_j^*}^{\alpha}[r] e^{j2\pi\alpha n} \quad (39)$$

where, for $r \in \{-1, 0, 1\}$,

$$\begin{aligned} \mathbf{R}_{\bar{\mathbf{y}}_j \bar{\mathbf{y}}_j^*}^{\alpha}[r] &\triangleq \left\langle \mathbf{R}_{\bar{\mathbf{y}}_j \bar{\mathbf{y}}_j^*}[n, r] e^{-j2\pi\alpha n} \right\rangle \\ &= \lim_{N \rightarrow +\infty} \frac{1}{2N+1} \sum_{n=-N}^N \mathbf{R}_{\bar{\mathbf{y}}_j \bar{\mathbf{y}}_j^*}[n, r] e^{-j2\pi\alpha n} \end{aligned} \quad (40)$$

is the *conjugate cyclic correlation matrix (CCCM)* at cycle frequency α and it is given by

$$\mathbf{R}_{\bar{\mathbf{y}}_j \bar{\mathbf{y}}_j^*}^{\alpha}[r] = \begin{cases} \Xi_{A,j,L,L}[r], & \alpha = 2\nu_{A,L}; \\ \Xi_{A,j,N,N}[r], & \alpha = 2\nu_{A,N}; \\ \Xi_{A,j,L,N}[r] + \Xi_{A,j,N,L}[r], & \alpha = \nu_{A,L} + \nu_{A,N}; \\ \mathbf{O}_{P \times P}, & \text{otherwise.} \end{cases} \quad (41)$$

It is worth noticing that there are three distinct cycle frequencies $2\nu_{A,L}$, $2\nu_{A,N}$, and $\nu_{A,L} + \nu_{A,N}$,⁸ which arise from linear combinations of the Doppler shifts $\nu_{A,L}$ and $\nu_{A,N}$. Thus, the cycle frequency set of (35) is

$$\mathcal{A} = \{2\nu_{A,L}, 2\nu_{A,N}, \nu_{A,L} + \nu_{A,N}\}. \quad (42)$$

Another key observation underlying our blind estimation approach is that, in practice, $\mathbf{R}_{\bar{\mathbf{y}}_j \bar{\mathbf{y}}_j^*}^{\alpha}[r]$ can be directly estimated from the received data using the consistent estimate (see, e.g., [61])

$$\hat{\mathbf{R}}_{\bar{\mathbf{y}}_j \bar{\mathbf{y}}_j^*}^{\alpha}[r] = \frac{1}{N_0} \sum_{n=0}^{N_0-1} \bar{\mathbf{y}}_j[n] \bar{\mathbf{y}}_j^T[n-r] e^{-j2\pi\alpha n}. \quad (43)$$

1) Blind estimation of the Doppler shifts

Estimation of the Doppler shifts $f_{A,L}$ and $f_{A,N}$ is equivalent to that of $\nu_{A,L}$ and $\nu_{A,N}$, respectively. For $j \in \{1, 2, \dots, J\}$, knowledge of the CCCMs $\mathbf{R}_{\bar{\mathbf{y}}_j \bar{\mathbf{y}}_j^*}^{\alpha}[-1]$, $\mathbf{R}_{\bar{\mathbf{y}}_j \bar{\mathbf{y}}_j^*}^{\alpha}[0]$, and $\mathbf{R}_{\bar{\mathbf{y}}_j \bar{\mathbf{y}}_j^*}^{\alpha}[1]$ enables one to blindly retrieve the unknown cycle frequency set (42) through the *one-dimensional* function:

$$\begin{aligned} J(\alpha) &\triangleq \sum_{j=1}^J \sum_{r=-1}^1 \left\| \mathbf{R}_{\bar{\mathbf{y}}_j \bar{\mathbf{y}}_j^*}^{\alpha}[r] \right\|^2 \\ &= \sum_{j=1}^J \sum_{r=-1}^1 \text{tr} \left(\mathbf{R}_{\bar{\mathbf{y}}_j \bar{\mathbf{y}}_j^*}^{\alpha}[r] \left\{ \mathbf{R}_{\bar{\mathbf{y}}_j \bar{\mathbf{y}}_j^*}^{\alpha}[r] \right\}^H \right), \end{aligned} \quad \text{with } \alpha \in [-1/2, 1/2). \quad (44)$$

By using differential calculus arguments, it can be shown that the function $J(\alpha)$ has three local maxima in $[-1/2, 1/2)$

⁸Since the LoS and NLoS components arrive at the BS from different angular directions, one can safely assume that $\nu_{A,L} \neq \nu_{A,N}$.

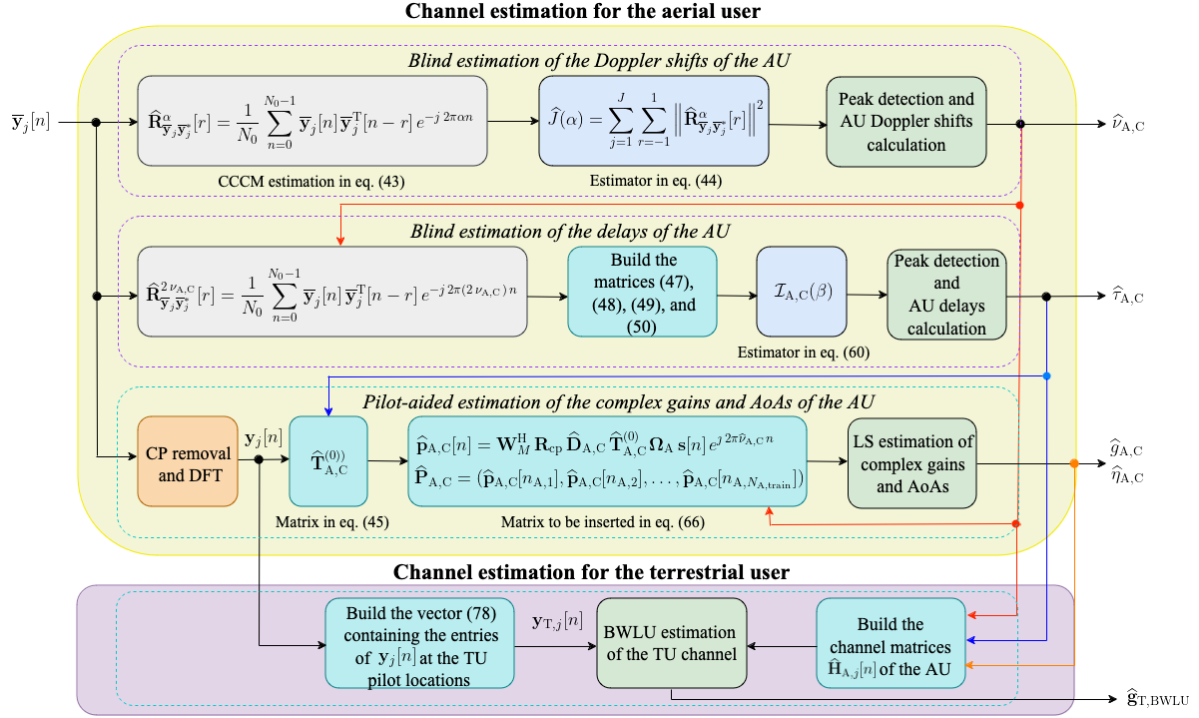


FIGURE 2. A summary of the proposed channel estimators for both the AU and TU (the BWLU estimator for the TU channel is depicted only).

$$\Xi_{A,j,C_1,C_2}[-1] \triangleq g_{A,C_1} e^{j\pi(j-1)\sin(\theta_{A,C_1})} g_{A,C_2} e^{j\pi(j-1)\sin(\theta_{A,C_2})} e^{j2\pi\nu_{A,C_2}} (\mathbf{D}_{A,C_1} \mathbf{T}_{A,C_1}^{(0)} \Omega_A) \Delta (\mathbf{D}_{A,C_2} \mathbf{T}_{A,C_2}^{(1)} \Omega_A)^T \quad (36)$$

$$\Xi_{A,j,C_1,C_2}[0] \triangleq g_{A,C_1} e^{j\pi(j-1)\sin(\theta_{A,C_1})} g_{A,C_2} e^{j\pi(j-1)\sin(\theta_{A,C_2})} \mathbf{D}_{A,C_1} [(\mathbf{T}_{A,C_1}^{(0)} \Omega_A) \Delta (\mathbf{T}_{A,C_2}^{(0)} \Omega_A)^T + (\mathbf{T}_{A,C_1}^{(1)} \Omega_A) \Delta (\mathbf{T}_{A,C_2}^{(1)} \Omega_A)^T] \mathbf{D}_{A,C_2} \quad (37)$$

$$\Xi_{A,j,C_1,C_2}[1] \triangleq g_{A,C_1} e^{j\pi(j-1)\sin(\theta_{A,C_1})} g_{A,C_2} e^{j\pi(j-1)\sin(\theta_{A,C_2})} e^{-j2\pi\nu_{A,C_2}} (\mathbf{D}_{A,C_1} \mathbf{T}_{A,C_1}^{(1)} \Omega_A) \Delta (\mathbf{D}_{A,C_2} \mathbf{T}_{A,C_2}^{(0)} \Omega_A)^T \quad (38)$$

at points $2\nu_{A,L}$, $2\nu_{A,N}$, and $\nu_{A,L} + \nu_{A,N}$. Hence, the cycle frequencies of the second-order ACS process (17) can be acquired by searching for the maxima of (44) over $[-1/2, 1/2)$, provided that $|\nu_{A,L}|, |\nu_{A,N}| \leq 1/4$. Specifically, if $\nu_{A,L} < \nu_{A,N}$, the maximum points of $J(\alpha)$ in $[-1/2, 1/2)$ are $2\nu_{A,L} < \nu_{A,L} + \nu_{A,N} < 2\nu_{A,N}$ in increasing order. On the contrary, if $\nu_{A,L} > \nu_{A,N}$, the increasing order of the maximum points is $2\nu_{A,L} < \nu_{A,L} + \nu_{A,N} < 2\nu_{A,L}$. Therefore, by picking up the smallest and largest maximum points of $J(\alpha)$ in $[-1/2, 1/2)$, one can acquire the Doppler shifts of the AU up to a permutation ambiguity, i.e., it is not possible to infer if the smallest (or, conversely, largest) maximum point of (44) is equal to $2\nu_{A,L}$ or $2\nu_{A,N}$. However, such an ambiguity is irrelevant for the detection process of the symbols transmitted by the AU.

In practice, the estimates of the Doppler shifts can be obtained from data by finding the peaks of the function $\hat{J}(\alpha)$ obtained from (44) by replacing (40) with (43).

2) Blind estimation of the time delays

Hereinafter, we assume that the Doppler shifts have been previously acquired as proposed in Subsection III-A-1 and, for the time being, they are assumed perfectly known.

The proposed estimation technique to acquire the delays $\tau_{A,L} = d_{A,L} T_c + \chi_{A,L}$ and $\tau_{A,N} = d_{A,N} T_c + \chi_{A,N}$ relies again on the AP conjugate correlation matrices $\mathbf{R}_{\bar{y}_j \bar{y}_j^*}[n, -1]$, $\mathbf{R}_{\bar{y}_j \bar{y}_j^*}[n, 0]$, and $\mathbf{R}_{\bar{y}_j \bar{y}_j^*}[n, 1]$ in (35). In addition, we capitalize on the following parameterization of the Toeplitz matrices $\mathbf{T}_{A,L}^{(b)}$ and $\mathbf{T}_{A,N}^{(b)}$ - defined in (18) with $b \in \{0, 1\}$ - in terms of the forward shift $\mathbf{F} \in \mathbb{R}^{P \times P}$ and backward shift $\mathbf{B} \in \mathbb{R}^{P \times P}$ matrices (see Subsection I-D):

$$\mathbf{T}_{A,C}^{(0)} = \sum_{\ell=0}^{L_{cp}} \psi(\ell T_c - \tau_{A,C}) \mathbf{F}^\ell \quad (45)$$

$$\mathbf{T}_{A,C}^{(1)} = \sum_{\ell=1}^{L_{cp}} \psi(\ell T_c - \tau_{A,C}) \mathbf{B}^{P-\ell} \quad (46)$$

for $C \in \{L, N\}$, where the pulse $\psi(t)$ is known at the BS.

Starting from the CCCMs (41), for $r \in \{-1, 0, 1\}$, at cycle frequency $\alpha = 2\nu_{A,C}$, which can be obtained from (36)–(38)

by setting $\mathbf{C}_1 = \mathbf{C}_2 = \mathbf{C} \in \{\mathbf{L}, \mathbf{N}\}$, we build the matrices

$$\begin{aligned} \Phi_{A,j,C}[-1] &\triangleq e^{-j2\pi\nu_{A,C}} \mathbf{D}_{A,C}^* \mathbf{R}_{\bar{\mathbf{y}}_j \bar{\mathbf{y}}_j^*}^{2\nu_{A,C}}[-1] \mathbf{D}_{A,C}^* \\ &= g_{A,C}^2 e^{j2\pi(j-1)\sin(\theta_{A,C})} \\ &\quad \cdot (\mathbf{T}_{A,C}^{(0)} \boldsymbol{\Omega}_A) \boldsymbol{\Delta} (\mathbf{T}_{A,C}^{(1)} \boldsymbol{\Omega}_A)^T \end{aligned} \quad (47)$$

$$\begin{aligned} \Phi_{A,j,C}[0] &\triangleq \mathbf{D}_{A,C}^* \mathbf{R}_{\bar{\mathbf{y}}_j \bar{\mathbf{y}}_j^*}^{2\nu_{A,C}}[0] \mathbf{D}_{A,C}^* \\ &= g_{A,C}^2 e^{j2\pi(j-1)\sin(\theta_{A,C})} \\ &\quad \cdot \left[(\mathbf{T}_{A,C}^{(0)} \boldsymbol{\Omega}_A) \boldsymbol{\Delta} (\mathbf{T}_{A,C}^{(0)} \boldsymbol{\Omega}_A)^T \right. \\ &\quad \left. + (\mathbf{T}_{A,C}^{(1)} \boldsymbol{\Omega}_A) \boldsymbol{\Delta} (\mathbf{T}_{A,C}^{(1)} \boldsymbol{\Omega}_A)^T \right] \end{aligned} \quad (48)$$

$$\begin{aligned} \Phi_{A,j,C}[1] &\triangleq e^{j2\pi\nu_{A,C}} \mathbf{D}_{A,C}^* \mathbf{R}_{\bar{\mathbf{y}}_j \bar{\mathbf{y}}_j^*}^{2\nu_{A,C}}[1] \mathbf{D}_{A,C}^* \\ &= g_{A,C}^2 e^{j2\pi(j-1)\sin(\theta_{A,C})} \\ &\quad \cdot (\mathbf{T}_{A,C}^{(1)} \boldsymbol{\Omega}_A) \boldsymbol{\Delta} (\mathbf{T}_{A,C}^{(0)} \boldsymbol{\Omega}_A)^T. \end{aligned} \quad (49)$$

The proposed estimation algorithm relies on the fact that

$$\begin{aligned} \Phi_{A,C} &\triangleq \sum_{j=1}^J \sum_{r=-1}^1 \Phi_{A,j,C}[r] \\ &= g_{A,C}^2 D_J^*(\sin(\theta_{A,C})) \mathbf{C}_{A,C} \boldsymbol{\Omega}_A \boldsymbol{\Delta} \boldsymbol{\Omega}_A^T \mathbf{C}_{A,C}^T \end{aligned} \quad (50)$$

for $\mathbf{C} \in \{\mathbf{L}, \mathbf{N}\}$, where the Dirichlet function has been defined in (2), the matrix $\mathbf{C}_{A,C} \triangleq \mathbf{T}_{A,C}^{(0)} + \mathbf{T}_{A,C}^{(1)} \in \mathbb{R}^{P \times P}$ is circulant by construction, whose first column is given by

$$\begin{aligned} \mathbf{c}_{A,C} &\triangleq \left(\psi(-\tau_{A,C}), \psi(T_c - \tau_{A,C}), \dots, \right. \\ &\quad \left. \psi(L_{cp} T_c - \tau_{A,C}), 0, \dots, 0 \right)^T. \end{aligned} \quad (51)$$

Such a circulant matrix can be easily diagonalized as

$$\mathbf{C}_{A,C} = \mathbf{W}_P \text{diag}(\mathbf{v}_{A,C}) \mathbf{W}_P^H \quad (52)$$

where the p th entry of

$$\mathbf{v}_{A,C} \triangleq \sqrt{P} \mathbf{W}_P^H \mathbf{c}_{A,C} \in \mathbb{C}^P \quad (53)$$

is given by $\{v_{A,C}\}_p = \Psi_{A,C}[p] e^{-j\frac{2\pi}{T_s} \tau_{A,C} p}$, with

$$\Psi_{A,C}[p] \approx \begin{cases} \frac{1}{T_c} \Psi\left(\frac{p}{T_s}\right), & \text{for } p \in \{0, 1, \dots, \frac{P}{2} - 1\} \\ \frac{1}{T_c} \Psi\left(\frac{p-P}{T_s}\right) e^{j\frac{2\pi}{T_s} \tau_{A,C} p}, & \text{for } p \in \{\frac{P}{2} - 1, \frac{P}{2}, \dots, P - 1\} \end{cases} \quad (54)$$

and $\Psi(f) \approx 0$ for $f \notin (-0.5/T_c, 0.5/T_c)$ being the Fourier transform of $\psi(t)$. Is is worth noticing that $\Psi_{A,C}[0], \Psi_{A,C}[1], \dots, \Psi_{A,C}[\frac{P}{2} - 1]$ are equal to the corresponding coefficients of the P -point DFT of $\psi(\ell T_c)$ and, thus, they are known at the BS.

To acquire the delay $\tau_{A,C}$, we observe that, by substituting (52) in (50), it results that

$$\begin{aligned} \mathbf{W}_P^H \Phi_{A,C} \mathbf{W}_P^* &= g_{A,C}^2 D_J^*(\sin(\theta_{A,C})) \\ &\quad \cdot \mathbf{E}_{A,C} \boldsymbol{\Psi}_{A,C} \boldsymbol{\Upsilon} \boldsymbol{\Psi}_{A,C} \mathbf{E}_{A,C} \end{aligned} \quad (55)$$

for $\mathbf{C} \in \{\mathbf{L}, \mathbf{N}\}$, where we have defined the matrices

$$\mathbf{E}_{A,C} \triangleq \text{diag}\left(1, e^{-j\frac{2\pi}{T_s} \tau_{A,C}}, \dots, e^{-j\frac{2\pi}{T_s} \tau_{A,C}(P-1)}\right) \quad (56)$$

$$\boldsymbol{\Psi}_{A,C} \triangleq \text{diag}(\Psi_{A,C}[0], \Psi_{A,C}[1], \dots, \Psi_{A,C}[P-1]) \quad (57)$$

$$\boldsymbol{\Upsilon} \triangleq \mathbf{W}_P^H \boldsymbol{\Omega}_A \boldsymbol{\Delta} \boldsymbol{\Omega}_A^T \mathbf{W}_P^* \in \mathbb{C}^{P \times P}. \quad (58)$$

For $p \in \{0, 1, \dots, P-1\}$, it is readily seen that the p th diagonal entry of $\mathbf{W}_P^H \Phi_{A,C} \mathbf{W}_P^*$ is given by

$$\begin{aligned} \{\mathbf{W}_P^H \Phi_{A,C} \mathbf{W}_P^*\}_{p,p} &= g_{A,C}^2 D_J^*(\sin(\theta_{A,C})) \Psi_{A,C}^2[p] \{\boldsymbol{\Upsilon}\}_{p,p} e^{-j\frac{4\pi}{T_s} \tau_{A,C} p}. \end{aligned} \quad (59)$$

At this point, let us introduce the *one-dimensional* cost function defined in (60) at the top of the next page, where $\Delta_{\max} \geq \max\{\tau_{A,L}, \tau_{A,N}\}$ is a known upper bound on the maximum delay of the AU channel. By resorting to the triangle inequality, it can be verified that, for $\mathbf{C} \in \{\mathbf{L}, \mathbf{N}\}$, $\mathcal{I}_{A,C}(\beta)$ takes its maximum value when $\beta = \tau_{A,C} + iT_s/2$ ($i \in \mathbb{Z}$). Hence, under the assumption $\Delta_{\max} < T_s/2$, acquisition of $\tau_{A,C}$ can be pursued by searching for the global maximum of (60) over the interval $[0, \Delta_{\max}] \subset [0, T_s/2)$.

In practice, an estimate $\hat{\tau}_{A,C}$ of the delay $\tau_{A,C}$ is derived by searching for the peak of the finite-sample version $\hat{\mathcal{I}}_{A,C}(\beta)$ of the cost function $\mathcal{I}_{A,C}(\beta)$ defined in (60), where $\hat{\mathcal{I}}_{A,C}(\beta)$ is obtained by replacing $\mathbf{R}_{\bar{\mathbf{y}}_j \bar{\mathbf{y}}_j^*}^{2\nu_{A,C}}[r]$ in (47)–(49), for $r \in \{-1, 0, 1\}$, with their corresponding estimates $\hat{\mathbf{R}}_{\bar{\mathbf{y}}_j \bar{\mathbf{y}}_j^*}^{2\nu_{A,C}}[r]$ [see (43)], evaluated at the estimated cycle frequency $2\hat{\nu}_{A,C}$ acquired through the algorithm in Subsection II-A-1.

B. Pilot-aided estimation of complex gain and AoA parameters

After acquiring the Doppler and delay parameters blindly, we propose to estimate the complex gain and AoA unknowns of the AU, by capitalizing on its pilots transmitted in the training intervals $\mathcal{N}_A = \{n_{A,1}, n_{A,2}, \dots, n_{A,N_{A,\text{train}}}\}$. For the present, Doppler and delay parameters are assumed to be perfectly known. The starting point of the pilot-aided estimation step is (22), which collects the signal received by the j -th antenna after CP removal and DFT.

For $n \in \mathcal{N}_A$ and $j \in \{1, 2, \dots, J\}$, it is convenient to rewrite (22) as follows

$$\begin{aligned} \mathbf{y}_j[n] &= g_{A,L} \eta_{A,L}^{j-1} \mathbf{p}_{A,L}[n] \\ &\quad + g_{A,N} \eta_{A,N}^{j-1} \mathbf{p}_{A,N}[n] + \mathbf{d}_{A,j}[n] \end{aligned} \quad (61)$$

where $\mathbf{p}_{A,C}[n] \triangleq \mathbf{W}_M^H \mathbf{R}_{cp} \mathbf{D}_{A,C} \mathbf{T}_{A,C}^{(0)} \boldsymbol{\Omega}_A \mathbf{s}_A[n] e^{j2\pi\nu_{A,C} n}$ is a *known* vector, $\eta_{A,C} \triangleq e^{j\pi \sin(\theta_{A,C})}$ is a complex parameter to be estimated together with $g_{A,C}$, for $\mathbf{C} \in \{\mathbf{L}, \mathbf{N}\}$, whereas $\mathbf{d}_{A,j}[n] \triangleq \mathbf{M}_{T,j} \mathbf{s}_T[n] + \mathbf{w}_j[n]$ represents disturbance from the AU viewpoint.

Given the AU symbol vector $\mathbf{s}_A[n]$, the random vector $\mathbf{y}_j[n]$ is circular, for $j \in \{1, 2, \dots, J\}$. By gathering all the training blocks received by the j -th antenna in the matrix $\mathbf{Y}_{A,j} \triangleq (\mathbf{y}_j[n_{A,1}], \mathbf{y}_j[n_{A,2}], \dots, \mathbf{y}_j[n_{A,N_{A,\text{train}}})) \in \mathbb{C}^{M \times N_{A,\text{train}}}$, one gets the compact matrix model

$$\mathbf{Y}_{A,j} = g_{A,L} \eta_{A,L}^{j-1} \mathbf{P}_{A,L} + g_{A,N} \eta_{A,N}^{j-1} \mathbf{P}_{A,N} + \mathbf{D}_{A,j} \quad (62)$$

$$\begin{aligned} \mathcal{I}_{A,C}(\beta) &\triangleq \left| \sum_{p=0}^{P/2-1} \{ \mathbf{W}_P^H \boldsymbol{\Phi}_{A,C} \mathbf{W}_P^* \}_{p,p} (\Psi_{A,C}^2[p])^* \{ \boldsymbol{\Upsilon} \}_{p,p}^* e^{j \frac{4\pi}{T_s} \beta p} \right| \\ &= |g_{A,C}|^2 |D_J^*(\sin(\theta_{A,C}))| \left| \sum_{p=0}^{P/2-1} |\Psi_{A,C}[p]|^4 |\{ \boldsymbol{\Upsilon} \}_{p,p}|^2 e^{-j \frac{4\pi}{T_s} (\tau_{A,C} - \beta) p} \right|, \quad \text{with } \beta \in [0, \Delta_{\max}] \end{aligned} \quad (60)$$

with

$$\mathbf{P}_{A,C} \triangleq (\mathbf{p}_{A,C}[n_{A,1}], \mathbf{p}_{A,C}[n_{A,2}], \dots, \mathbf{p}_{A,C}[n_{A,N_{A,\text{train}}}] \in \mathbb{C}^{M \times N_{A,\text{train}}} \quad (63)$$

$$\mathbf{D}_{A,j} \triangleq (\mathbf{d}_{A,j}[n_{A,1}], \mathbf{d}_{A,j}[n_{A,2}], \dots, \mathbf{d}_{A,j}[n_{A,N_{A,\text{train}}}] \in \mathbb{C}^{M \times N_{A,\text{train}}} \quad (64)$$

for $C \in \{L, N\}$ and $j \in \{1, 2, \dots, J\}$. From now on, it is assumed that $\eta_{A,L}$ is distinct from $\eta_{A,N}$.

Since the correlation properties of $\mathbf{D}_{A,j}$ are unknown due to the multiple access interference arising from the transmission of the TU, estimation strategies involving the second-order statistics of the disturbance, such as best linear unbiased (BLU) or linear MMSE estimators, cannot be implemented in this case. Therefore, we resort to the *least-squares (LS)* criterion [63] to acquire channel gains and AoAs of the AU, whose salient feature is that no probability assumptions are made about the received data.

The four parameters $\eta_{A,L}$, $g_{A,L}$, $\eta_{A,N}$, and $g_{A,N}$ have to be estimated. The LS estimator is defined as

$$(\hat{g}_{A,L}, \hat{g}_{A,N}, \hat{\eta}_{A,L}, \hat{\eta}_{A,N}) = \arg \min_{\substack{\rho_L, \rho_N \in \mathbb{C} \\ |\varrho_L| = |\varrho_N| = 1}} \mathcal{L}_A(\rho_L, \rho_N, \varrho_L, \varrho_N) \quad (65)$$

with

$$\mathcal{L}_A(\rho_L, \rho_N, \varrho_L, \varrho_N) \triangleq \sum_{j=1}^J \left\| \mathbf{Y}_{A,j} - \sum_{C \in \{L, N\}} \rho_C \varrho_C^{j-1} \mathbf{P}_{A,C} \right\|^2. \quad (66)$$

Significant computational savings follow from the observation that, for any *given* $\eta_{A,L}$ and $\eta_{A,N}$, the problem of finding the LS estimates of $g_{A,L}$ and $g_{A,N}$, corresponding to that $\eta_{A,L}$ and $\eta_{A,N}$, are obtained by solving the 2×2 linear system:

$$\frac{\partial}{\partial \rho_L^*} \mathcal{L}_A(\rho_L, \rho_N, \varrho_L, \varrho_N) = -\Lambda_{L,0} + \Lambda_{L,1} \rho_L + \Lambda_{L,2} \rho_N = 0 \quad (67)$$

$$\frac{\partial}{\partial \rho_N^*} \mathcal{L}_A(\rho_L, \rho_N, \varrho_L, \varrho_N) = -\Lambda_{N,0} + \Lambda_{N,1} \rho_N + \Lambda_{N,2} \rho_L = 0 \quad (68)$$

with

$$\Lambda_{C,0} \triangleq \sum_{j=1}^J \text{tr} \left(\mathbf{Y}_{A,j} \mathbf{P}_{A,C}^H \eta_{A,C}^{-(j-1)} \right) \quad (69)$$

$$\Lambda_{C,1} \triangleq J \text{tr}(\mathbf{P}_{A,C} \mathbf{P}_{A,C}^H) = J \|\mathbf{P}_{A,C}\|^2 \quad (70)$$

$$\Lambda_{C,2} \triangleq \sum_{j=1}^J \text{tr} \left(\mathbf{P}_{A,\bar{C}} \mathbf{P}_{A,C}^H (\eta_{A,\bar{C}} \eta_{A,C}^*)^{j-1} \right) \quad (71)$$

where $\bar{C} = N$ when $C = L$, whereas $\bar{C} = L$ when $C = N$. The solution of the system (67)-(68) is given by

$$\hat{g}_{A,L} = \frac{\Lambda_{L,0} \Lambda_{N,1} - \Lambda_{L,2} \Lambda_{N,0}}{\Lambda_{L,1} \Lambda_{N,1} - \Lambda_{L,2} \Lambda_{N,2}} \quad (72)$$

$$\hat{g}_{A,N} = \frac{\Lambda_{L,1} \Lambda_{N,0} - \Lambda_{L,0} \Lambda_{N,2}}{\Lambda_{L,1} \Lambda_{N,1} - \Lambda_{L,2} \Lambda_{N,2}}. \quad (73)$$

By substituting (72)-(73) into (65), the LS estimates of $\eta_{A,L}$ and $\eta_{A,N}$ can be found by

$$(\hat{\eta}_{A,L}, \hat{\eta}_{A,N}) = \arg \min_{|\varrho_L| = |\varrho_N| = 1} \mathcal{L}_A(\hat{g}_{A,L}, \hat{g}_{A,N}, \varrho_L, \varrho_N). \quad (74)$$

In general, the cost function in (74) is multimodal. However, there exist computationally-efficient global optimization procedures, which try to provide an efficiently global optimization by partition of definition space at multi-scale levels, see, e.g., [64], [65]. Such methods have a stable convergence speed and the optimization solution is independent of the selection of initial solutions [64].

In practice, the previously obtained estimates of the Doppler and delay parameters (see Subsection III-A-1 and III-A-2) have to be used for LS acquisition of the complex gain and AoA unknowns of the AU. Specifically, the LS problem to be solved comes from replacing $\mathbf{P}_{A,C}$ in (66) with its corresponding estimate $\hat{\mathbf{P}}_{A,C} \triangleq (\hat{\mathbf{p}}_{A,C}[n_{A,1}], \hat{\mathbf{p}}_{A,C}[n_{A,2}], \dots, \hat{\mathbf{p}}_{A,C}[n_{A,N_{A,\text{train}}}]$, where $\hat{\mathbf{p}}_{A,C}[n] \triangleq \mathbf{W}_M^H \mathbf{R}_{\text{cp}} \hat{\mathbf{D}}_{A,C} \hat{\mathbf{T}}_{A,C}^{(0)} \boldsymbol{\Omega}_A \mathbf{s}_A[n] e^{j 2\pi \hat{\nu}_{A,C} n}$, for any $n \in \mathcal{N}_A$, and $\hat{\mathbf{T}}_{A,C}^{(0)}$ is built from (45) by using $\hat{\tau}_{A,C}$ in lieu of $\tau_{A,C}$.

C. Computational issues

With reference to Fig. 2, the computational complexity of the overall estimation algorithm for the AU is mainly dominated by the first block devoted to the Doppler shifts acquisition, i.e., the CCCM estimation. In particular, the CCCM estimation entails $\mathcal{O}(N_0^2 P^2 J)$ floating point operations (flops) and, thus, the complexity burden quadratically grows with the length N_0 of the observation interval.

D. NOMA is used by TUs in the uplink

So far, we have assumed that the TUs transmit to the BS using the OMA scheme. We now discuss how the proposed channel estimation algorithm for the AU will work if nonorthogonal RBs are assigned to TUs in the uplink.

In this scenario, a single AU may send noncircular symbols using the same RBs shared by a group of static TUs

that concurrently transmit to the BS by employing a power-domain NOMA scheme with circular modulation formats. In such a case, the proposed blind estimation procedure of Doppler and delay parameters is unaffected, since the terrestrial transmissions do not contribute to the CCCM (41) due to the modulation and Doppler diversities. On the other hand, the uplink signals of the TUs appear in the disturbance term $\mathbf{d}_{A,j}[n]$ in (61), thus impacting on the pilot-aided estimation of complex gain and AoA parameters. However, existing schemes in the power-domain NOMA literature (e.g., [45], [66]) creates multiple groups, each with one “weak” TU at the cell edge and one “strong” TU at the cell center. For such a NOMA scheme, the power of $\mathbf{d}_{A,j}[n]$ will be mainly dictated by the strong TU and, hence, compared with the single TU case considered in this paper, the performance degradation of the proposed LS estimator (65) will be negligible.

IV. Channel estimation for the terrestrial user

The estimation of the AU channel follows an array signal processing approach, where the parameters characterizing the AU channel are estimated. We resort to a completely different approach for the estimation of the TU channel. More precisely, the TU channel estimator passes to the SIC detector the diagonal time-invariant matrix $\mathbf{H}_{T,j} \equiv \mathbf{M}_{T,j}$, for each antenna index $j \in \{1, 2, \dots, J\}$. Since the TU channel is time invariant, we pursue a pilot-aided approach for estimating $\mathbf{M}_{T,j}$, which relies on the Q_T pilot symbols transmitted by the TU at the subcarriers $\mathcal{M}_T = \{m_{T,0}, m_{T,1}, \dots, m_{T,Q_T-1}\}$ during the $N_{T,\text{train}}$ symbol intervals $\mathcal{N}_T = \{n_{T,1}, n_{T,2}, \dots, n_{T,N_{T,\text{train}}}\}$. This task is developed by assuming perfect knowledge of the AU channel matrices $\mathbf{H}_{A,1}[n], \mathbf{H}_{A,2}[n], \dots, \mathbf{H}_{A,J}[n]$, which can be acquired as proposed in Section III. To this aim, according to (25), instead of separately estimating the parameters (i.e., time delays, AoAs, and channel gains) characterizing the TU channel, we choose to directly estimate the vector

$$\mathbf{g}_{T,j} \triangleq \sum_{k=1}^{K_T} \mathbf{g}_{T,j,k} \in \mathbb{C}^{L_{\text{cp}}} \quad (75)$$

which gathers all the aggregated state information of the TU channel corresponding to the j th receiving antenna.

Let us consider the frequency-domain received data given by (22). Denoting by

$$\mathbf{y}_{T,j}[n] \triangleq (y_j^{[L_{\text{cp}}+m_{T,0}]}[n], y_j^{[L_{\text{cp}}+m_{T,1}]}[n], \dots, y_j^{[L_{\text{cp}}+m_{T,Q_T-1}]}[n])^T \in \mathbb{C}^{Q_T} \quad (76)$$

$$\mathbf{w}_{T,j}[n] \triangleq (w_j^{[L_{\text{cp}}+m_{T,0}]}[n], w_j^{[L_{\text{cp}}+m_{T,1}]}[n], \dots, w_j^{[L_{\text{cp}}+m_{T,Q_T-1}]}[n])^T \in \mathbb{C}^{Q_T} \quad (77)$$

the vectors containing the entries of $\mathbf{y}_j[n]$ and $\mathbf{w}_j[n]$ at the TU pilot locations, respectively, we get

$$\mathbf{y}_{T,j}[n] = \mathbf{P}_T[n] \mathbf{g}_{T,j} + \mathbf{d}_{T,j}[n] \quad (78)$$

for $n \in \mathcal{N}_T$ and $j \in \{1, 2, \dots, J\}$, where

$$\mathbf{P}_T[n] \triangleq \sqrt{M} \mathbf{S}_T([n]) \mathbf{W}_M^H \mathbf{L} \in \mathbb{C}^{Q_T \times L_{\text{cp}}} \quad (79)$$

is a *known* matrix, with the pilot matrix $\mathbf{S}_T([n]) \in \mathbb{C}^{Q_T \times M}$ obtained by picking up the rows of $\text{diag}(\mathbf{s}_T[n])$ at positions $\{m_{T,0} + 1, m_{T,1} + 1, \dots, m_{T,Q_T-1} + 1\}$ for $n \in \mathcal{N}_T$, whereas $\mathbf{d}_{T,j}[n] \triangleq \mathbf{M}_{A,j}[n] \mathbf{s}_A[n] + \mathbf{w}_j[n]$ represents disturbance from the TU viewpoint, with $\mathbf{M}_{A,j}[n] \in \mathbb{C}^{Q_T \times M}$ obtained by taking the rows of the known matrix $\mathbf{H}_{A,j}[n]$ corresponding to the indexes $\{m_{T,0} + 1, m_{T,1} + 1, \dots, m_{T,Q_T-1} + 1\}$. The training blocks received by the j -th antenna for $n \in \mathcal{N}_T$ are gathered into the $(Q_T N_{T,\text{train}})$ -dimensional complex vector

$$\mathbf{y}_{T,j} \triangleq (\mathbf{y}_{T,j}^T[n_{T,1}], \mathbf{y}_{T,j}^T[n_{T,2}], \dots, \mathbf{y}_{T,j}^T[n_{T,N_{T,\text{train}}}]^T)^T \quad (80)$$

thus yielding, for $j \in \{1, 2, \dots, J\}$,

$$\mathbf{y}_{T,j} = \mathbf{P}_T \mathbf{g}_{T,j} + \mathbf{d}_{T,j} \quad (81)$$

where

$$\mathbf{P}_T \triangleq (\mathbf{P}_T^T[n_{T,1}], \mathbf{P}_T^T[n_{T,2}], \dots, \mathbf{P}_T^T[n_{T,N_{T,\text{train}}}]^T)^T \in \mathbb{C}^{(Q_T N_{T,\text{train}}) \times L_{\text{cp}}} \quad (82)$$

$$\mathbf{d}_{T,j} \triangleq (\mathbf{d}_{T,j}^T[n_{T,1}], \mathbf{d}_{T,j}^T[n_{T,2}], \dots, \mathbf{d}_{T,j}^T[n_{T,N_{T,\text{train}}}]^T)^T \in \mathbb{C}^{Q_T N_{T,\text{train}}} \quad (83)$$

Finally, we collect the data received by all the antennas of the BS into $\mathbf{y}_T \triangleq (\mathbf{y}_{T,1}^T, \mathbf{y}_{T,2}^T, \dots, \mathbf{y}_{T,J}^T)^T \in \mathbb{C}^{J Q_T N_{T,\text{train}}}$, thus yielding the vector signal model

$$\mathbf{y}_T = (\mathbf{I}_J \otimes \mathbf{P}_T) \mathbf{g}_T + \mathbf{d}_T \quad (84)$$

where

$$\mathbf{g}_T \triangleq (\mathbf{g}_{T,1}^T, \mathbf{g}_{T,2}^T, \dots, \mathbf{g}_{T,J}^T)^T \in \mathbb{C}^{J L_{\text{cp}}} \quad (85)$$

$$\mathbf{d}_T \triangleq (\mathbf{d}_{T,1}^T, \mathbf{d}_{T,2}^T, \dots, \mathbf{d}_{T,J}^T)^T \in \mathbb{C}^{J Q_T N_{T,\text{train}}} \quad (86)$$

We assume that \mathbf{P}_T is full-column rank, i.e., $\text{rank}(\mathbf{P}_T) = L_{\text{cp}}$ and $Q_T N_{T,\text{train}} \geq L_{\text{cp}}$, which ensures that \mathbf{g}_T is uniquely identifiable from (84) in the absence of the disturbance \mathbf{d}_T .

There are different estimation strategies that can be pursued to estimate the TU channel from (84). We focus on estimators belonging to the family of the classical estimation approaches [63], for which \mathbf{g}_T is viewed as deterministic but unknown vector. The simplest estimator is represented by the LS one (see, e.g., [63]):

$$\begin{aligned} \hat{\mathbf{g}}_{T,\text{LS}} &\triangleq \arg \min_{\mathbf{g}_T \in \mathbb{C}^{J L_{\text{cp}}}} \|\mathbf{y}_T - \mathbf{P}_T \mathbf{g}_T\|^2 \\ &= \left[\mathbf{I}_J \otimes (\mathbf{P}_T^H \mathbf{P}_T)^{-1} \mathbf{P}_T^H \right] \mathbf{y}_T \end{aligned} \quad (87)$$

which does not exploit the CSI knowledge of the AU and, thus, performs poorly in a NOMA setting (see Section V). On the other hand, the BS can jointly exploits the knowledge of the AU channel matrices $\mathbf{H}_{A,1}[n], \mathbf{H}_{A,2}[n], \dots, \mathbf{H}_{A,J}[n]$ and the noncircularity of the AU symbols, by resorting to the *best WL unbiased (BWL) estimator*, which is restricted

to be WL in the data, it is unbiased, and it has minimum variance. In matrix form, a WL estimator is defined by

$$\begin{aligned} \hat{\mathbf{g}}_T &= \mathbf{A}_1 \mathbf{y}_T + \mathbf{A}_2 \mathbf{y}_T^* \\ &= \underbrace{(\mathbf{A}_1, \mathbf{A}_2)}_{\mathbf{A} \in \mathbb{C}^{(JL_{cp}) \times (2JQ_T N_{T,train})}} \underbrace{\begin{pmatrix} \mathbf{y}_T \\ \mathbf{y}_T^* \end{pmatrix}}_{\tilde{\mathbf{y}}_T \in \mathbb{C}^{2JQ_T N_{T,train}}} = \mathbf{A} \tilde{\mathbf{y}}_T \end{aligned} \quad (88)$$

where $\mathbf{A}_1, \mathbf{A}_2 \in \mathbb{C}^{(JL_{cp}) \times (JQ_T N_{T,train})}$ and

$$\tilde{\mathbf{y}}_T = \tilde{\mathbf{P}}_T \mathbf{g}_T + \mathbf{J}_{JQ_T N_{T,train}} \tilde{\mathbf{P}}_T^* \mathbf{g}_T^* + \tilde{\mathbf{d}}_T \quad (89)$$

with

$$\tilde{\mathbf{P}}_T \triangleq (\mathbf{I}_J \otimes \mathbf{P}_T^T, \mathbf{O}_{(JQ_T N_{T,train}) \times (JL_{cp})}^T)^T \in \mathbb{C}^{(2JQ_T N_{T,train}) \times (JL_{cp})} \quad (90)$$

$\mathbf{J}_{JQ_T N_{T,train}} \in \mathbb{R}^{(2JQ_T N_{T,train}) \times (2JQ_T N_{T,train})}$ defined in (1), and, finally, $\tilde{\mathbf{d}}_T \triangleq (\mathbf{d}_T^T, \mathbf{d}_T^H)^T \in \mathbb{C}^{2JQ_T N_{T,train}}$. It is readily verified that $\tilde{\mathbf{d}}_T$ has zero mean, i.e., $\mathbb{E}(\tilde{\mathbf{d}}_T) = \mathbf{0}_{2JQ_T N_{T,train}}$, and

$$\mathbf{R}_{\tilde{\mathbf{d}}_T \tilde{\mathbf{d}}_T} \triangleq \mathbb{E}(\tilde{\mathbf{d}}_T \tilde{\mathbf{d}}_T^H) = \tilde{\mathbf{M}}_A \tilde{\mathbf{M}}_A^H + \sigma_w^2 \mathbf{I}_{2JQ_T N_{T,train}} \quad (91)$$

where

$$\tilde{\mathbf{M}}_A \triangleq \begin{pmatrix} \mathbf{M}_A \\ \mathbf{M}_A^* [\mathbf{I}_{N_{T,train}} \otimes \Delta] \end{pmatrix} \in \mathbb{C}^{(2JQ_T N_{T,train}) \times (MN_{T,train})} \quad (92)$$

with

$$\begin{aligned} \mathbf{M}_A &\triangleq (\mathbf{M}_{A,1}^T, \mathbf{M}_{A,2}^T, \dots, \mathbf{M}_{A,J}^T)^T \in \mathbb{C}^{(JQ_T N_{T,train}) \times (MN_{T,train})} \\ \mathbf{M}_{A,j} &\triangleq \text{diag}(\mathbf{M}_{A,j}[n_{T,1}], \mathbf{M}_{A,j}[n_{T,2}], \dots, \mathbf{M}_{A,j}[n_{T,N_{T,train}}]) \end{aligned} \quad (93)$$

The key point of the proposed BWLU estimation approach is the fact that the correlation matrix $\mathbf{R}_{\tilde{\mathbf{d}}_T \tilde{\mathbf{d}}_T}$ is known at the BS after acquiring the AU channel state (see Section III).

According to (89), in order for $\hat{\mathbf{g}}_T$ to be unbiased, we require $\mathbb{E}(\hat{\mathbf{g}}_T) = \mathbf{A} \mathbb{E}(\tilde{\mathbf{y}}_T) = \mathbf{g}_T$, which is tantamount to imposing the unbiased constraint

$$\mathbf{A} \underbrace{\begin{pmatrix} \mathbf{I}_J \otimes \mathbf{P}_T & \mathbf{O}_{(JQ_T N_{T,train}) \times (JL_{cp})} \\ \mathbf{O}_{(JQ_T N_{T,train}) \times (JL_{cp})} & \mathbf{I}_J \otimes \mathbf{P}_T^* \end{pmatrix}}_{\mathbf{\Pi}_T \in \mathbb{C}^{(2JQ_T N_{T,train}) \times (2JL_{cp})}} = \underbrace{(\mathbf{I}_{JL_{cp}}, \mathbf{O}_{(JL_{cp}) \times (JL_{cp})})}_{\mathbf{\Theta} \in \mathbb{R}^{(JL_{cp}) \times (2JL_{cp})}} \quad (94)$$

The BWLU estimator is found by minimizing the variance at the estimator output

$$\begin{aligned} \text{Var}(\hat{\mathbf{g}}_T) &\triangleq \mathbb{E}(\|\hat{\mathbf{g}}_T - \mathbf{g}_T\|^2) \\ &= \text{tr}[\mathbf{A} \mathbb{E}(\tilde{\mathbf{y}}_T \tilde{\mathbf{y}}_T^H) \mathbf{A}^H] - \|\mathbf{g}_T\|^2 \\ &= \text{tr}(\mathbf{A} \mathbf{R}_{\tilde{\mathbf{d}}_T \tilde{\mathbf{d}}_T} \mathbf{A}^H) \end{aligned} \quad (95)$$

where we have also taken into account the constraint (94). The classical approach for minimizing (95) subject to the unbiased constraint (94) is the method of Lagrange multipliers, which yields the solution (see, e.g., [63])

$$\hat{\mathbf{g}}_{T,BWLU} = \mathbf{\Theta} \left(\mathbf{\Pi}_T^H \mathbf{R}_{\tilde{\mathbf{d}}_T \tilde{\mathbf{d}}_T}^{-1} \mathbf{\Pi}_T \right)^{-1} \mathbf{\Pi}_T^H \mathbf{R}_{\tilde{\mathbf{d}}_T \tilde{\mathbf{d}}_T}^{-1} \tilde{\mathbf{y}}_T \quad (96)$$

whose corresponding minimum variance is given by

$$\text{Var}(\hat{\mathbf{g}}_{T,BWLU}) = \text{tr} \left[\mathbf{\Theta} \left(\mathbf{\Pi}_T^H \mathbf{R}_{\tilde{\mathbf{d}}_T \tilde{\mathbf{d}}_T}^{-1} \mathbf{\Pi}_T \right)^{-1} \mathbf{\Theta}^H \right]. \quad (97)$$

It can be verified by direct inspection that

$$\begin{aligned} \mathbf{A}_{BWLU} &= \mathbf{\Theta} \left(\mathbf{\Pi}_T^H \mathbf{R}_{\tilde{\mathbf{d}}_T \tilde{\mathbf{d}}_T}^{-1} \mathbf{\Pi}_T \right)^{-1} \mathbf{\Pi}_T^H \mathbf{R}_{\tilde{\mathbf{d}}_T \tilde{\mathbf{d}}_T}^{-1} \\ &= (\mathbf{A}_{BWLU,1}, \mathbf{A}_{BWLU,2}) \end{aligned} \quad (98)$$

with $\mathbf{A}_{BWLU,2} \neq \mathbf{O}_{(JL_{cp}) \times (JQ_T N_{T,train})}$: in this case, the BWLU estimator is expected to outperform its BLU counterpart in the minimum-variance sense.

In practice, the BWLU estimator is built by using estimates $\hat{\mathbf{H}}_{A,1}[n], \hat{\mathbf{H}}_{A,2}[n], \dots, \hat{\mathbf{H}}_{A,J}[n]$ of the AU channel matrices $\mathbf{H}_{A,1}[n], \mathbf{H}_{A,2}[n], \dots, \mathbf{H}_{A,J}[n]$, which are obtained through the three-step approach proposed in Section III. Such an estimator is implemented by replacing $\mathbf{R}_{\tilde{\mathbf{d}}_T \tilde{\mathbf{d}}_T}$ in (96) with its corresponding estimate $\hat{\mathbf{R}}_{\tilde{\mathbf{d}}_T \tilde{\mathbf{d}}_T}$ coming from $\hat{\mathbf{H}}_{A,1}[n], \hat{\mathbf{H}}_{A,2}[n], \dots, \hat{\mathbf{H}}_{A,J}[n]$, for $n \in \mathcal{N}_T$.

A. Computational issues

With reference to Fig. 2, the computational complexity of the estimation algorithm for the TU is mainly dominated by the second block of the channel acquisition for the TU, i.e., the BWLU estimation. In particular, the BWLU estimation relies on the inversion of the matrix $\mathbf{R}_{\tilde{\mathbf{d}}_T \tilde{\mathbf{d}}_T}$ which entails $\mathcal{O}(J^3 Q_T^3 N_{T,train}^3)$ flops if one resorts to batch algorithms. Such a matrix inversion can also be implemented by means of a simple and effective recursion, similar to the well-known recursive least square algorithm, with a complexity per iteration of order only $\mathcal{O}(J^2 Q_T^2 N_{T,train}^2)$ flops. Anyway, the complexity burden is independent of the length N_0 of the observation interval.

B. NOMA is used by TUs in the uplink

As in Subsection III-D, we discuss herein how the proposed channel estimation algorithms for the TU will be employed when the BS assigns to a single AU the same RBs shared by a group of power-domain NOMA TUs.

If the BS uses orthogonal pilot sequences to distinguish different power-domain NOMA TUs [67], then the received signal from a given TU can be obtained by performing the correlation of the received data with the pilot sequence of the desired TU. After performing this preprocessing for each user, the estimators (87) or (96) will be used with minor modifications to individually estimate the channel of each TU. On the other hand, if the BS allocates the same pilot to the power-domain NOMA TUs, the estimators (87) or (96) will estimate a linear combination of the channels from all NOMA TUs. Such an estimate will still provide a useful description of the combined channel, which could be exploited by the BS to beamform a combination of the data symbols intended for the NOMA TUs [66].

V. Numerical results

In this section, we provide numerical results aimed at evaluating the performance of the proposed channel estimators for the SG-NOMA scheme. To this aim, we consider the following simulation setting. The AU and TU employ OFDM modulation with $M = 16$ subcarriers, CP of length $L_{cp} = 4$, sampling rate $1/T_c = 625$ kHz. The signaling format of the AU is a $\pi/2$ -BPSK. On the other hand, the TU transmits quaternary-phase-shift-keying (QPSK) symbols. The carrier frequency is set to $f_{carrier} = 27$ GHz. Regarding the training protocol, we set $Q_T = 16$ and $N_{A,train} = N_{T,train} = 80$. Unless otherwise specified, the TU coherence time is equal to $N_{coh} = 16.384$ OFDM ksymbols.

The ULA at the BS has $J = 4$ antennas. The number of paths of the TU-to-BS link is fixed to $K_T = 2$. The Rician factor of the AU channel is $K_A = 6$ dB. The direction cosines $\sin(\theta_{A,L})$ and $\sin(\theta_{A,N})$ associated with the AoA at the BS are independent random variables uniformly distributed into $[0, 1]$. The generic time delay $\tau \in \{\tau_{T,1}, \tau_{T,2}, \tau_{A,L}, \tau_{A,N}\}$ of the TU and AU channels is randomly generated according to the one-sided exponentially decreasing delay power spectrum [9], i.e.,

$$\tau = -\tau_{slope} \ln \left[1 - u \left(1 - e^{-\Delta_{max}/\tau_{slope}} \right) \right] \quad (99)$$

where $\Delta_{max} = 3T_c$, the slope-time is $\tau_{slop} = 2T_c$, and u is a random variable uniformly distributed into $[0, 1]$. Unless otherwise specified, we assume that the constant radial speed of the AU is $v = 8$ m/s, $f_{max} = 720$ Hz, and the AoD $\vartheta_{A,L}$ and $\vartheta_{A,N}$ are independent random variables uniformly distributed into $[0, \pi]$. The power relationship between the AU and TU at the BS is measured by the *aerial-to-terrestrial ratio* (ATR) defined as

$$ATR \triangleq \frac{\sigma_{A,L}^2 + \sigma_{A,N}^2}{\sum_{k=1}^{K_T} \sigma_{g_{T,k}}^2} \quad (100)$$

whereas the signal-to-noise ratio is given by

$$SNR \triangleq \frac{\sigma_{A,L}^2 + \sigma_{A,N}^2}{\sigma_w^2}. \quad (101)$$

In each one of the 400 Monte Carlo runs, a new set of symbols, noise and channel parameters for both the AU and TU are randomly generated. Regarding the estimation of the channel parameters of the AU (see Section III), we calculate the arithmetic mean of the MSEs of the Doppler shifts $f_{A,L}$ and $f_{A,N}$ (normalized by f_{max}^2), the time delays $\tau_{A,L}$ and $\tau_{A,N}$ (normalized by Δ_{max}^2), the channel gains $g_{A,L}$ and $g_{A,N}$ (normalized by $\sigma_{A,L}^2$), and the direction cosines $\sin(\theta_{A,L})$ and $\sin(\theta_{A,N})$. With reference to the estimation of the TU channel (see Section IV), we report the estimator output (95) (normalized by $\sum_{k=1}^{K_T} \sigma_{g_{T,k}}^2$). As baseline channel estimation schemes, we report the OMA-based counterparts of the proposed estimators, which are implemented by orthogonalizing pilot symbols in the frequency domain, i.e., we set $\mathcal{M}_A \equiv \{0, 1, \dots, 7\}$ and $\mathcal{M}_T \equiv \{8, 9, \dots, 15\}$ in each training symbol interval.

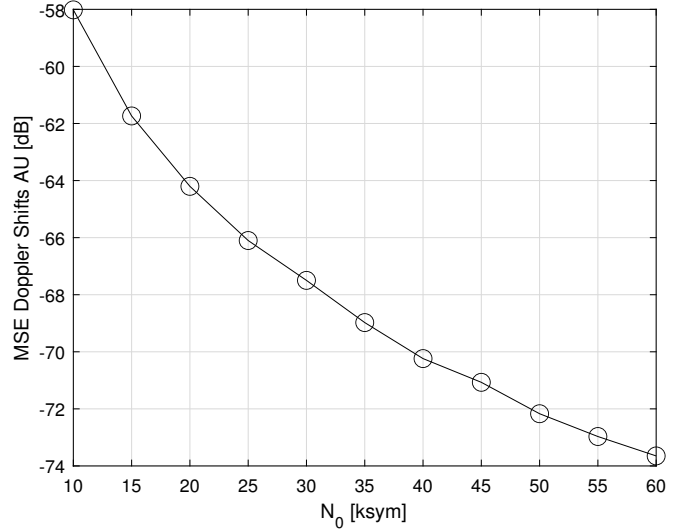


FIGURE 3. MSE of the AU Doppler shifts versus the length N_0 of the observation interval, (ATR = 0 dB and SNR = 14 dB).

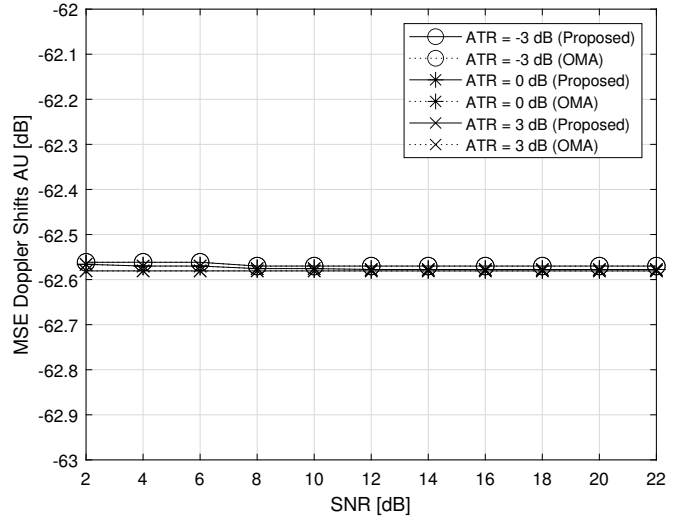


FIGURE 4. MSE of the AU Doppler shifts versus SNR and ATR values.

Figs. 3–7 depict the estimation performance of the proposed finite-sample estimators outlined in Section III for the AU channel parameters (i.e., Doppler shifts, time delays, channel gains, and AoAs). Generally, it is apparent that such estimators exhibit satisfactory MSE performance for all the considered SNR and ATR values.

Fig. 3 reports the MSE of the Doppler shifts as a function of the length N_0 of the observation interval (in OFDM symbols). As expected, the estimation accuracy rapidly improves as N_0 increases, thus demonstrating that the proposed blind estimator of the Doppler shifts is asymptotically consistent. Remarkably, Fig. 4 shows that the MSE of the Doppler shifts is independent of both the SNR and ATR, achieving the value -62.57 dB approximately. Such an invariance with respect to both the SNR and ATR comes from the fact that the blind estimator proposed in Subsection III-A-1 relies on the second-order conjugate cyclic statistics of the received

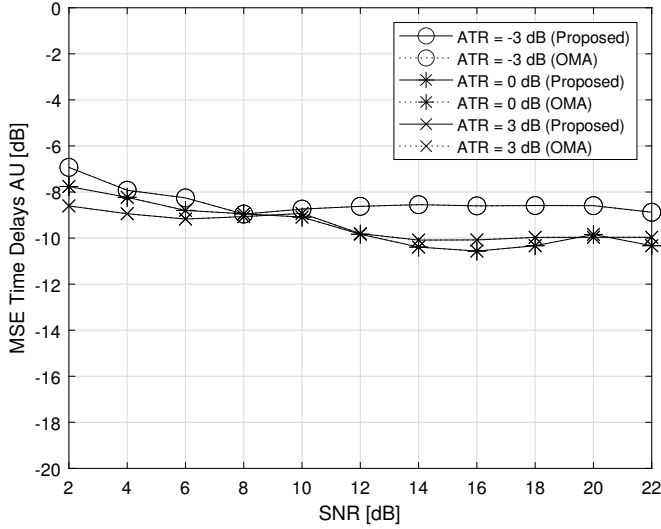


FIGURE 5. MSE of the AU time delays versus SNR and ATR values.

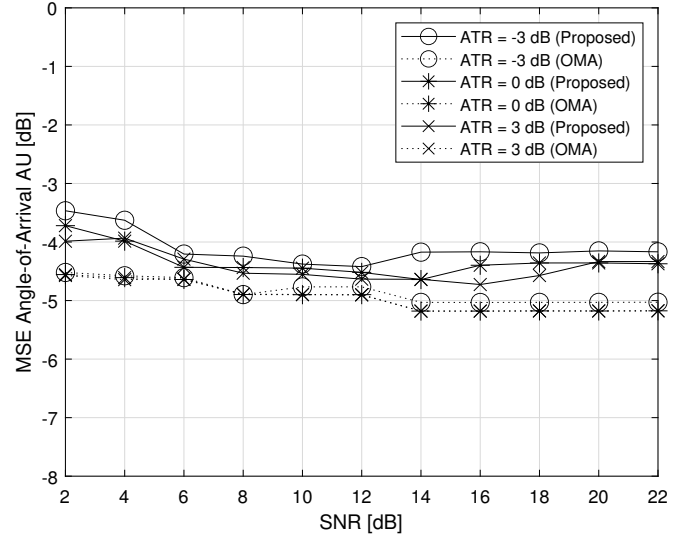


FIGURE 7. MSE of the AU directive cosines versus SNR and ATR values.

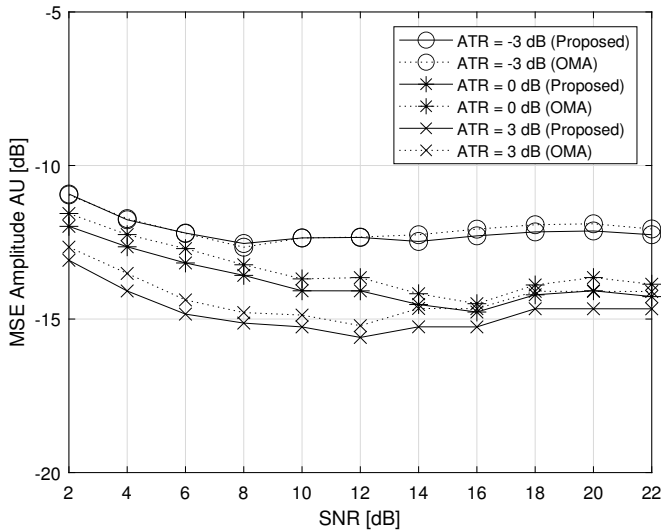


FIGURE 6. MSE of the AU channel gains versus SNR and ATR values.

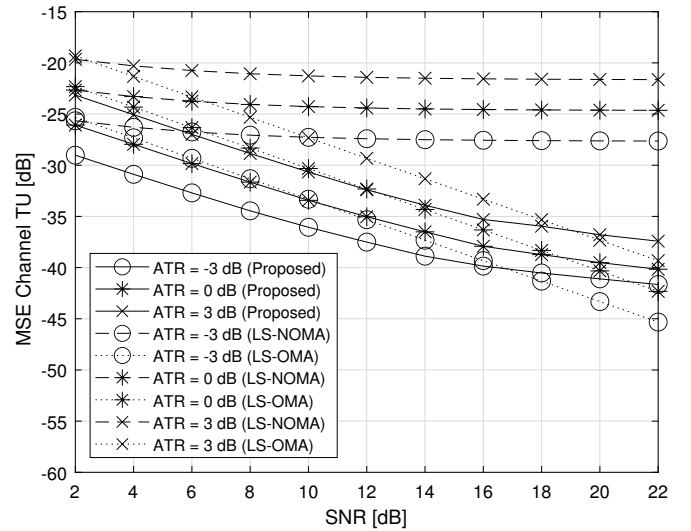


FIGURE 8. MSE of TU channel versus SNR and ATR values (dashed line for the LS-NOMA estimator, solid line for the BWLU estimator, and dotted line for the LS-OMA estimator).

data, for which the contribution of the circular wide-sense stationary TU signal and noise is negligible for sufficiently large (but finite) values of N_0 .

We remember that, as the Doppler shifts, the time delays are blindly estimated by using the conjugate second-order statistics of the ACS random process (17). In this case, a weak dependence of the MSE on the SNR and ATR values can be observed in Fig. 5, which is due to the fact that the estimates of the time delays in Subsection III-A-2 also feel the aftereffects of the estimation error of the cycle frequency acquired previously. Estimation errors due to finite sample-size effects (i.e., when the conjugate second-order statistics are estimated from a finite number of samples) depend on both the SNR and ATR in a nonlinear manner [68], thus contributing to the fluctuations of the curves in Fig. 5. However, the variability of the MSE of the time delays is confined in a range of about 1 dB as a function of the SNR

and the MSE curves translate down of nearly 1 dB further to an ATR reduction of 3 dB. It is worth noticing that the performance of the proposed NOMA-based estimators in Figs. 4 and 5 is almost indistinguishable from that of the corresponding OMA-based counterparts, thus corroborating the high robustness of the proposed Doppler shifts and time delays estimation approaches against the interference caused by the TU.

The MSE of the channel amplitudes in Fig. 6 also exhibits a weak dependence on the SNR and ATR values. However, the additional exploitation of the pilot symbols allows to achieve MSE values smaller than -10 dB for $\text{SNR} > 2$ dB, even when the ATR is as low as -3 dB. In contrast, the MSE of the AoAs in Fig. 7 is actually independent of the ATR, thus further corroborating the robustness of the proposed

pilot-based estimators developed in Subsection III-B against the interference generated by the TU. With respect to Figs. 4 and 5, fluctuations in the MSE curves of channel amplitudes in Fig. 6 and AoAs in Fig. 7 become even more evident since, although the corresponding estimation procedures are based on a LS approach that does not involve estimation of statistics, these estimators suffer of the error propagation phenomenon that is inherent of the proposed multi-stage estimation approach (see Fig. 2), according to which the existence of estimation error in a given stage will deteriorate the estimation accuracy in the next stage. Such an error propagation prevents the LS estimates of channel amplitudes and AoAs from monotonically decreasing for increasing values of SNR and/or ATR. The proposed NOMA-based estimators and their corresponding OMA-based counterparts in Figs. 6 and 7 exhibit slight performance differences. In particular, the performance of OMA-based estimators gets slightly worse than that of the corresponding NOMA-based counterparts in the case of amplitude AU estimation. This behavior is due to the fact that amplitude estimation procedures are typically very sensitive to the number of available pilot symbols. Indeed, as a consequence of the orthogonalization of pilot symbols in the frequency domain, OMA-based estimators count on a reduced number of pilot symbols, compared to NOMA-based estimation algorithms.

Fig. 8 depicts the MSE performance of the TU channel estimator proposed in Section IV. Besides the MSE of the BWLU estimator (96) (solid line), we also report the MSE of the simpler LS-NOMA estimator (87) (dashed line). As predicted by our analysis, the BWLU estimator largely outperforms the LS-NOMA one since it additionally exploits the CSI knowledge of the AU. This demonstrates the importance of firstly estimate the channel parameters of the AU and, then, using the obtained estimates to acquire the CSI of the TU. As a matter of fact, the performance curves of the OMA-based LS estimator (dotted line) are monotonically decreasing functions of the SNR, whereas the MSE performance of the corresponding NOMA-based counterparts exhibits a floor in the high SNR regime, which is due to the residual interference from the AU transmission.

Finally, Tab. 1 reports the MSE performance of all the estimation algorithms under comparison for different value of the radial speed v of the AU. It can be inferred that the radial speed of the AU has a negligible effect on the estimates, except for the estimated values of the AoA of the AU, whose accuracy improves for increasing value of v .

VI. Conclusions and directions for future work

In this paper, we have considered the scenario where a flying AU is paired with a static TU through power-domain uplink NOMA. Despite many existing works, we have investigated the performance of finite-sample channel estimation procedures. We have shown that blind and pilot-aided techniques can be suitably combined to accurately estimate the AU and TU channel that are characterized by different second-order

wide-sense properties in both the ACS (or Doppler) and modulation domains. Specifically, the AU mobility induces ACS features in the signal received from sky due to Doppler effects that are not present in the signal received from ground, provided that the TU is static. Moreover, the AU can employ a noncircular modulation format, as opposed to the TU that transmits circular symbols. We have demonstrated that Doppler shifts and time delays of the AU can be estimated blindly with high accuracy that is basically independent of the TU and noise powers. The remaining AU parameters, i.e., channel gains and AoAs, can be instead estimated through a pilot-assisted LS approach that exploits the previously acquired knowledge of the Doppler shifts and time delays of the AU. By equipping the BS with the CSI knowledge of the AU, the overall channel of the TU can be subsequently acquired through a high-precision pilot-based BWLU estimator.

The performance of the proposed estimators has been corroborated through Monte Carlo numerical results. In this respect, an interesting research subject consists of theoretically investigating the consistency and asymptotic distribution of such algorithms. Another appealing research issue is to extend our framework to the case in which TUs also communicate with the BS according to a NOMA scheme.

Appendix

In BPSK modulation, the symbols $\{b_A[n]\}$ are modeled as a sequence of i.i.d. real-valued random variables, each assuming equiprobable values in $\{\pm 1\}$. A variation of BPSK is $\pi/2$ -BPSK modulation scheme [49]–[51], wherein two sets of BPSK constellations are shifted by $\pi/2$, i.e.,

$$s_A[n] = e^{j\frac{\pi}{4}} e^{j\frac{\pi}{2}[n]_2} b_A[n]. \quad (102)$$

It can be readily verified that $\mathbb{E}(|s_A[n]|^2) = 1$ and $\mathbb{E}(s_A^2[n]) = j(-1)^n$. Consequently, under the standard assumption that the number of subcarriers M is even, one has $\mathbb{E}(s_A[n] s_A^H[n]) = \mathbf{I}_M$, whereas $\mathbb{E}(s_A[n] s_A^T[n]) = \mathbf{\Delta}$, with $\mathbf{\Delta} \triangleq j \text{diag}(1, -1, 1, \dots, -1) \in \mathbb{C}^{M \times M}$.

REFERENCES

- [1] Y. Zeng, J. Lyu, and R. Zhang, "Cellular-connected UAV: potential, challenges, and promising technologies," *IEEE Wireless Commun.*, vol. 26, pp. 120–127, Feb. 2019.
- [2] Y. Zeng, Q. Wu, and R. Zhang, "Accessing from the sky: A tutorial on UAV communications for 5G and Beyond," *Proc. IEEE*, vol. 107, pp. 2327–2375, Dec. 2019.
- [3] W. Mei and R. Zhang, "Aerial-ground interference mitigation for cellular-connected UAV," *IEEE Wireless Commun.*, vol. 28, pp. 167–173, Feb. 2021.
- [4] X. Lin *et al.*, "The sky is not the limit: LTE for unmanned aerial vehicles," *IEEE Commun. Magazine*, vol. 56, pp. 204–210, Apr. 2018.
- [5] W.K. New, C.Y. Leow, K. Navaie, Y. Sun, and Z. Ding, "Application of NOMA for cellular-connected UAVs: Opportunities and challenges," *Sci. China Inf. Sci.*, vol. 64, pp. 1–14, Apr. 2021.
- [6] Nokia. (Oct. 2016). *F-Cell Technology From Nokia Bell Labs Revolutionizes Small Cell Deployment By Cutting Wires, Costs and Time*. [Online]. Available: <https://www.nokia.com/about-us/news/releases/2016/10/03/f-cell-technology-from-nokia-bell-labsrevolutionizes-small-cell-deployment-by-cutting-wires-costs-and-time/>

TABLE 1. MSEs of AU and TU channel parameters for different values of the radial speed of the AU [dB].

v [m/s]	Doppler Shifts AU		Time Delays AU		Amplitude AU		AoA AU		Channel TU		
	Proposed	OMA	Proposed	OMA	Proposed	OMA	Proposed	OMA	Proposed	LS-NOMA	LS-OMA
2	-62.8159	-62.8159	-11.2695	-11.2695	-16.2791	-15.7644	-2.7585	-3.9616	-37.4665	-24.9258	-34.1684
4	-62.6253	-62.6253	-10.8137	-10.8137	-15.9419	-15.7462	-3.3521	-4.5738	-37.1741	-24.5377	-34.2129
8	-62.5776	-62.5776	-10.3907	-10.3907	-14.5273	-14.1755	-4.6412	-5.1795	-36.5062	-24.5013	-34.3215
16	-62.5230	-62.5230	-9.7083	-9.7083	-12.8208	-12.5091	-6.7672	-6.0224	-35.2183	-24.3936	-34.8025

- [7] Huawei. (Nov. 2017). *Digital Sky Initiative*. [Online]. Available: <https://www.huawei.com/en/industry-insights/outlook/mobilebroadband/xlabs/industry-views/digital-sky-initiative>
- [8] R. Amer, W. Saad, H. ElSawy, M.M. Butt, and N. Marchetti, "Caching to the sky: Performance analysis of cache-assisted CoMP for cellular-connected UAVs," in *Proc. IEEE Wireless Commun. Netw. Conf. (WCNC)*, Apr. 2019, pp. 1-6.
- [9] E. Haas, "Aeronautical channel modeling," *IEEE Trans. Veh. Technol.*, vol. 51, pp. 254-264, Mar. 2002.
- [10] B. Van Der Bergh, A. Chiumento, and S. Pollin, "LTE in the sky: Trading off propagation benefits with interference costs for aerial nodes," *IEEE Commun. Magazine*, vol. 54, pp. 44-50, May 2016.
- [11] L. Afonso, N. Souto, P. Sebastiao, M. Ribeiro, T. Tavares, and R. Marinheiro, "Cellular for the skies: Exploiting mobile network infrastructure for low altitude air-to-ground communications," *IEEE Aersp. Electron. Syst. Mag.*, vol. 31, pp. 4-11, Aug. 2016.
- [12] H.C. Nguyen, R. Amorim, J. Wigard, I.Z. Kovács, T.B. Sørensen, and P.E. Mogensen, "How to ensure reliable connectivity for aerial vehicles over cellular networks," *IEEE Access*, vol. 6, pp. 12304-12317, 2018.
- [13] Z. Xue, J. Wang, Q. Shi, G. Ding, and Q. Wu, "Time-frequency scheduling and power optimization for reliable multiple UAV communications," *IEEE Access*, vol. 6, pp. 3992-4005, 2018.
- [14] M.M. Azari, F. Rosas, and S. Pollin, "Cellular connectivity for UAVs: Network modeling, performance analysis, and design guidelines," *IEEE Trans. Wireless Commun.*, vol. 18, pp. 3366-3381, July 2019.
- [15] P. Chandhar and E.G. Larsson, "Massive MIMO for connectivity with drones: Case studies and future directions," *IEEE Access*, vol. 7, pp. 94676-94691, 2019.
- [16] G. Geraci, A. Garcia-Rodriguez, L. Galati Giordano, D. López-Pérez, and E. Björnson, "Understanding UAV cellular communications: From existing networks to massive MIMO," *IEEE Access*, vol. 6, pp. 67853-67865, 2018.
- [17] R. Amer, W. Saad, and N. Marchetti, "Toward a connected sky: Performance of beamforming with down-tilted antennas for ground and UAV user co-existence," *IEEE Commun. Lett.*, vol. 23, pp. 1840-1844, Oct. 2019.
- [18] U. Challita, W. Saad and C. Bettstetter, "Interference management for cellular-connected UAVs: A deep reinforcement learning approach," *IEEE Trans. Wireless Commun.*, vol. 18, pp. 2125-2140, Apr. 2019.
- [19] U. Challita, A. Ferdowsi, M. Chen, and W. Saad, "Machine learning for wireless connectivity and security of cellular-connected UAVs," *IEEE Trans. Wireless Commun.*, vol. 26, pp. 28-35, Feb. 2019.
- [20] Z. Ding *et al.*, "Application of non-orthogonal multiple access in LTE and 5G networks," *IEEE Commun. Mag.*, vol. 55, pp. 185-191, Feb. 2017.
- [21] W. Shin, M. Vaezi, B. Lee, D.J. Love, J. Lee, and H.V. Poor, "Non-orthogonal multiple access in multi-cell networks: Theory, performance, and practical challenges," *IEEE Commun. Mag.*, vol. 55, pp. 176-183, Oct. 2017.
- [22] S.M.R. Islam, N. Avazov, O.A. Dobre, and K.-S. Kwak, "Power-domain non-orthogonal multiple access (NOMA) in 5G systems: Potentials and challenges," *IEEE Commun. Surveys Tuts.*, vol. 19, pp. 721-742, 2nd Quart. 2017.
- [23] H. Sari, F. Vanhaverbeke, and M. Moeneclaey, "Multiple access using two sets of orthogonal signal waveforms," *IEEE Commun. Lett.*, vol. 4, pp. 4-6, Jan. 2000.
- [24] Z. Ding, Z. Yang, P. Fan, and H.V. Poor, "On the performance of non-orthogonal multiple access in 5G systems with randomly deployed users," *IEEE Signal Process. Lett.*, vol. 21, pp. 1501-1505, Dec. 2014.
- [25] Z. Wei, L. Yang, D.W.K. Ng, J. Yuan, and L. Hanzo, "On the performance gain of NOMA over OMA in uplink communication systems," *IEEE Trans. Commun.*, vol. 68, pp. 536-568, Jan. 2020.
- [26] S.K. Zaidi, S.F. Hasan, and X. Gui, "Outage analysis of ground-aerial NOMA with distinct instantaneous channel gain ranking," *IEEE Trans. Veh. Technol.*, vol. 68, pp. 10775-10790, Nov. 2019.
- [27] W.K. New, C.Y. Leow, K. Navaie, and Z. Ding, "Robust non-orthogonal multiple access for aerial and ground users," *IEEE Trans. Wireless Commun.*, vol. 19, pp. 4793-4805, July 2020.
- [28] W. Mei and R. Zhang, "Cooperative NOMA for downlink asymmetric interference cancellation," *IEEE Wireless Commun. Lett.*, vol. 9, pp. 884-888, June 2020.
- [29] W. Mei and R. Zhang, "Uplink cooperative NOMA for cellular-connected UAV," *IEEE J. Select. Topics Signal Process.*, vol. 13, pp. 644-656, June 2019.
- [30] X. Mu, Y. Liu, L. Guo, and J. Lin, "Non-orthogonal multiple access for air-to-ground communication," *IEEE Trans. Commun.*, vol. 68, pp. 2934-2949, May 2020.
- [31] N. Senadhira, S. Durrani, X. Zhou, N. Yang, and M. Ding, "Uplink NOMA for cellular-connected UAV: Impact of UAV trajectories and altitude," *IEEE Trans. Commun.*, vol. 68, pp. 5242-5258, Aug. 2020.
- [32] X. Pang *et al.*, "Uplink precoding optimization for NOMA cellular-connected UAV networks," *IEEE Trans. Commun.*, vol. 68, pp. 1271-1283, Feb. 2020.
- [33] R. Hadani *et al.*, "Orthogonal time frequency space (OTFS) modulation for millimeter-wave communications systems," in *IEEE MTT-S Int. Microw. Symp. Dig.*, June 2017, pp. 681-683.
- [34] Z. Ding, R. Schober, P. Fan, and H.V. Poor, "OTFS-NOMA: An Efficient Approach for Exploiting Heterogenous User Mobility Profiles," *IEEE Trans. Commun.*, vol. 67, pp. 7950-7965, Nov. 2019.
- [35] Z. Ding, "Robust beamforming design for OTFS-NOMA," *IEEE Open J. Commun. Soc.*, vol. 1, pp. 33-40, 2020.
- [36] A. Thomas, K. Deka, P. Raviteja and S. Sharma, "Convolutional sparse coding based channel estimation for OTFS-SCMA in uplink," *IEEE Trans. Commun.*, vol. 70, pp. 5241-5257, Aug. 2022.
- [37] S.P. Muppaneni, S.R. Mattu, and A. Chockalingam, "Channel and radar parameter estimation with fractional delay-Doppler using OTFS," *IEEE Commun. Lett.*, vol. 27, pp. 1392-1396, May 2023.
- [38] P. Raviteja, K.T. Phan, and Y. Hong, "Embedded pilot-aided channel estimation for OTFS in delay-Doppler channels," *IEEE Trans. Veh. Technol.*, vol. 68, pp. 4906-4917, May 2019.
- [39] J. Hu, Z. Bai, H. Xu, H. Liu, Y. Wang, and K. Kwak, "Cross-domain channel estimation based serial interference cancellation in NOMA-OTFS system," *IEEE Commun. Lett.*, Early Access, 2024.
- [40] W. A. Gardner, *Introduction to Random Processes*. New York: McGraw-Hill, 1990.
- [41] B. Picinbono and P. Chevalier, "Widely linear estimation with complex data," *IEEE Trans. Signal Process.*, vol. 43, pp. 2030-2033, Aug. 1995.
- [42] A. Hjørungnes and D. Gesbert, "Complex-valued matrix differentiation: techniques and key results," *IEEE Trans. Signal Process.*, vol. 55, pp. 2740-2746, June 2007.
- [43] R.A. Horn and C.R. Johnson, *Matrix Analysis*. New York: Cambridge Univ. Press, 1990.
- [44] *NR; Physical Channels and Modulation (Release 15)*, document TS 38.211, 3GPP, 2019.
- [45] Z. Ding, P. Fan, and H.V. Poor, "Impact of user pairing on 5G nonorthogonal multiple-access downlink transmissions," *IEEE Trans. Veh. Technol.*, vol. 65, pp. 6010-6023, Aug. 2016.
- [46] C. Kosta, B. Hunt, A.U. Qudus, and R. Tafazolli, "On interference avoidance through inter-cell interference coordination (ICIC) based on OFDMA mobile systems," *IEEE Commun. Surveys Tuts.*, vol. 15, pp. 973-995, 3rd Quart. 2013.

- [47] A.S. Hamza, S.S. Khalifa, H.S. Hamza, and K. Elsayed, "A survey on inter-cell interference coordination techniques in OFDMA-based cellular networks," *IEEE Commun. Surveys Tuts.*, vol. 15, pp. 1642-1670, 4th Quart. 2013.
- [48] P.J. Schreier and L.L. Scharf, *Statistical Signal Processing of Complex-valued Data: The Theory of Improper and Noncircular Signals*. Cambridge (UK), Cambridge University Press, 2010.
- [49] 3GPP, "Physical channels and modulation," 3rd Generation Partnership Project (3GPP), TS 38.211 V 15.5.0, Mar. 2019.
- [50] 3GPP, "Physical layer procedures for data," 3rd Generation Partnership Project (3GPP), TS 38.213 V 15.5.0, Mar. 2019.
- [51] IITH et al., "Comparison of $\pi/2$ BPSK with and without frequency domain pulse shaping: Results with PA model," 3GPP TSG-RAN WG1 Ad-Hoc NR Meeting, R1-1701180, Spokane, WA, USA, 2017.
- [52] T. Rappaport, *Wireless Communications: Principles and Practice*, 2nd ed. Upper Saddle River, NJ, USA: Prentice-Hall, 2001.
- [53] A. Napolitano, *Generalizations of Cyclostationary Signal Processing: Spectral Analysis and Application*. John Wiley & Sons, Ltd. – IEEE Press, 2012.
- [54] W.G. Newhall et al., "Wideband air-to-ground radio channel measurements using an antenna array at 2 GHz for low-altitude operations," in *Proc. IEEE Mil. Commun. Conf. (MILCOM)*, Boston, MA, USA, 2003, pp. 1422-1427.
- [55] V. Va, J. Choi, and R.W. Heath, "The impact of beamwidth on temporal channel variation in vehicular channels and its implications," *IEEE Trans. Veh. Technol.*, vol. 66, pp. 5014-5029, Jun. 2017.
- [56] J.G. Proakis, *Digital Communications*. New York, NY, USA: McGraw-Hill, 2001.
- [57] ITU, "Propagation Data and Prediction Methods Required for the Design of Terrestrial Broadband Radio Access Systems Operating in a Frequency Range From 3 to 60 GHz", International Telecommunication Union (ITU), document Rec. P.1410-5, Feb. 2012.
- [58] N. Cherif, M. Alzenad, H. Yanikomeroglu, and A. Yongacoglu, "Downlink coverage and rate analysis of an aerial user in vertical heterogeneous networks (VHetNets)," *IEEE Trans. Wireless Commun.*, vol. 20, pp. 1501-1516, March 2021.
- [59] J. Holis and P. Pechac, "Elevation dependent shadowing model for mobile communications via high altitude platforms in built-up areas," *IeeeTAP*, vol. 56, pp. 1078-1084, Apr. 2008.
- [60] C. Corduneanu, *Almost Periodic Functions*. Chelsea Publishing Company New York, 1989.
- [61] A.V. Dandawaté and G.B. Giannakis, "Asymptotic theory of mixed time averages and k th-order cyclic moment and cumulant statistics," *IEEE Trans. Inf. Theory*, vol. 41, pp. 216-232, Jan. 1995.
- [62] P. Ciblat, P. Loubaton, E. Serpedin, and G.B. Giannakis, "Performance analysis of blind carrier frequency offset estimators for noncircular transmissions through frequency-selective channels," *IEEE Trans. Signal Process.*, vol. 50, pp. 130-140, Jan. 2002.
- [63] S.M. Kay, *Fundamentals of Statistical Signal Processing: Estimation Theory*. Englewood Cliffs, NJ: Prentice-Hall, 1993.
- [64] W. Sun and Y. Dong, "Study of multiscale global optimization based on parameter space partition," *J. Glob. Optim.*, vol. 49, pp. 149-172, Jan. 2011.
- [65] M.J. Kochenderfer and T.A. Wheeler, *Algorithms for Optimization*. The MIT Press, 2019.
- [66] H.V. Cheng, E. Björnson, and E.G. Larsson, "Performance analysis of NOMA in training-based multiuser MIMO systems," *IEEE Trans. Wireless Commun.*, vol. 17, pp. 372-385, Jan. 2018.
- [67] D. Fan, F. Gao, G. Wang, Z. Zhong, and A. Nallanathan, "Channel estimation and transmission strategy for hybrid mmwave NOMA systems," *IEEE J. Select. Topics Signal Process.*, vol. 13, pp. 584-596, June 2019.
- [68] F. Li, H. Liu, and R.J. Vaccaro, "Performance analysis for DOA estimation algorithms: Unification, simplification, and observations," *IEEE Trans. Aerosp. Electron. Syst.*, vol. 29, pp. 1170-1184, Oct. 1993.



Donatella Darsena (Senior Member, IEEE) received the Dr. Eng. degree *summa cum laude* in telecommunications engineering in 2001, and the Ph.D. degree in electronic and telecommunications engineering in 2005, both from the University of Napoli Federico II, Italy. From 2001 to 2002, she worked as embedded system designer in the Telecommunications, Peripherals and Automotive Group, STMicroelectronics, Milano, Italy. In 2005 she joined the Department of Engineering at Parthenope University of Napoli, Italy and worked

first as an Assistant Professor and then as an Associate Professor from 2005 to 2022. She is currently an Associate Professor in the Department of Electrical Engineering and Information Technology of the University of Napoli Federico II, Italy. Her research interests are in the broad area of signal processing for communications, with current emphasis on reflected-power communications, orthogonal and nonorthogonal multiple access techniques, wireless system optimization, and physical-layer security. Dr. Darsena has served as a Senior Editor for IEEE ACCESS since 2024, Executive Editor for IEEE COMMUNICATIONS LETTERS since 2023, and Associate Editor for IEEE SIGNAL PROCESSING LETTERS since 2020. She was an Associate Editor of IEEE ACCESS (from 2018 to 2023), of IEEE COMMUNICATIONS LETTERS (from 2016 to 2019), and Senior Area Editor of IEEE COMMUNICATIONS LETTERS (from 2020 to 2023).



Ivan Iudice received the B.S. and M.S. degrees in telecommunications engineering in 2008 and 2010, respectively, and the Ph.D. degree in information technology and electrical engineering in 2017, all from University of Napoli Federico II, Italy.

Since November 2011, he has been with the Italian Aerospace Research Centre (CIRA), Capua, Italy. He first served as part of the Electronics and Communications Laboratory and he is currently part of the Security Unit. He is involved in several international projects. He serves as reviewer for several international journals and as TPC member for several international conferences. He is author of several papers on refereed journals and international conferences. His research activities mainly lie in the area of signal and array processing for communications, with current interests focused on physical-layer security, space-time techniques for cooperative communications systems and reconfigurable metasurfaces.



Francesco Verde (Senior Member, IEEE) received the Dr. Eng. degree *summa cum laude* in electronic engineering from the Second University of Napoli, Italy, in 1998, and the Ph.D. degree in information engineering from the University of Napoli Federico II, in 2002. Since December 2002, he has been with the University of Napoli Federico II, Italy. He first served as an Assistant Professor of signal theory and mobile communications and, since December 2011, he has served as an Associate Professor of telecommunications with

the Department of Electrical Engineering and Information Technology. His research activities include reflected-power communications, orthogonal/non-orthogonal multiple-access techniques, wireless systems optimization, and physical-layer security.

Prof. Verde has been involved in several technical program committees of major IEEE conferences in signal processing and wireless communications. He has served as Associate Editor for IEEE TRANSACTIONS ON VEHICULAR TECHNOLOGY since 2022. He was an Associate Editor of the IEEE TRANSACTIONS ON SIGNAL PROCESSING (from 2010 to 2014), IEEE SIGNAL PROCESSING LETTERS (from 2014 to 2018), IEEE TRANSACTIONS ON COMMUNICATIONS (from 2017 to 2022), and Senior Area Editor of the IEEE SIGNAL PROCESSING LETTERS (from 2018 to 2023), as well as Guest Editor of the EURASIP Journal on Advances in Signal Processing in 2010 and SENSORS MDPI in 2018-2022.